STRUCTURAL INVESTIGATIONS ON SOME MOLECULAR COMPOUNDS OF BIOMEDICAL INTEREST

O. COZAR[1,2*], V. CHIŞ[1], I.B. COZAR[3], N. VEDEANU[44]

Abstract. *Experimental FT-IR, Raman, SERS, NMR, EPR and theoretical DFT studies on pharmaceutical compounds as metoclopramide, paroxetine, amlodipine, pindolol, verapamil, metoprolol and metal complexes of Pd(II) with theophylline and Cu(II) with ^{15}N- lysine or ^{15}N-ornithine are reported. The optimized molecular structure, molecular electrostatic potential (MEP) and experimental vibrational spectra were assigned according to DFT calculations, B3LYP/6-31G(D) level of theory, in order to establish their electrophilic attack and nucleophilic reactions positions, the adsorption geometry to the silver colloidal nanoparticles and also the hydrogen bonding interactions. The elucidation of the interaction mode of metal ions with aminoacids and theophylline are significant as models for metalloproteins and also to the coordinations with major constituents of DNA and RNA. The most stable conformes, protonated and neutral forms of molecular species corresponding to a local minimum potential energy were also established.*

Keywords: biomedical compounds, spectroscopic methods, DFT calculations

Introduction

Various experimental techniques (X-ray diffraction, FT-IR, Raman, NMR, EPR) and quantum chemical calculations were shown to be very useful for structural characterization of biomedical compounds, and for a good understanding of their pharmacological activity [1–3].

Since different conformations or enantiomers of such molecules can drastically influence their physico-chemical behavior and pharmacological activity, the knowledge of their structures is of utmost importance.

From the experimental methods, Raman scattering offers important structural information making it a powerful molecular investigation tool. When the molecules are adsorbed to rough metal surfaces the Raman cross section is enhanced several orders of magnitude and analytes in the micro-molar

[1]Babeş-Bolyai University, Faculty of Physics, RO-400084, Cluj-Napoca, Romania.
[2]Academy of Romanian Scientists, Splaiul Independenţei 54, RO-050094, Bucharest, Romania.
[*](onuc.cozar@phys.ubbcluj.ro)
[3]National Institute for Research and Development of Isotopic and Molecular Technologies, 65-103 Donath, 400293 Cluj-Napoca, Romania.
[4]Iuliu Hatieganu University of Medicine and Pharmacy, Faculty of Pharmacy, RO-400023,Cluj-Napoca, Romania.

concentration can be investigated [4,5]. The potential to combine high sensitivity with substantial structural information content makes from surface-enhanced Raman scattering (SERS) spectroscopy a powerful tool in a variety of fields, including also biospectroscopy [6,7].

For a proper understanding of the experimental spectra, density functional theory (DFT) methods [8] have been shown to be successful in predicting various molecular properties, giving results of a quality comparable or even better than highly correlated ab initio techniques for a substantially less computational cost. In the framework of DFT approach, the hybrid exchange–correlation B3LYP functional [9] and the standard split valence basis set 6-31G(d) is one of the most used since it proved its ability in reproducing various molecular properties, including vibrational and NMR spectra.

This theoretical method at B3LYP/6-31G(d) level of theory was success fully used by us to obtain the optimized geometries and subtile informations about the electronic structure of the investigated molecules [10-12].

Molecular electrostatic potential (MEP) is related to the electronic density and is a very useful descriptor in understanding sites for electrophilic attack and nucleophilic reactions as well as hydrogen bonding interactions [13, 14]. MEPs are also well suited for analyzing processes based on the ”recognition” of one molecule by another, as in drug–receptor, and enzyme–substrate interaction, because it is through their potentials that the two species first ‘‘see’’ each other [15].

The structural results on some biomedical compounds obtained by experimental FT-IR, Raman, SERS, NMR, EPR spectroscopies and density functional theory (DFT) are present in this paper.

In the first part, the structural aspects on farmaceutical compounds as metoclopramide, paroxetine, amlodipine, pindolol, verapamil and metoprolol used to combat the nausea that occurs in the treatment with anticancer agents, to treat major depression, anxiety, blood pressure, angina pectoris and other cardiovascular diseases were investigated. The results obtained on novel compounds with antibacterial potential synthesized at the Faculty of Pharmacy, Cluj-Napoca are also presented here.

In the second part the coordination mode of theophylline and 2,2’ – bipyridyne at Pd(II) ion is analysed by IR, ^{1}H-NMR and theoretical methods. Theophylline is important for establish the interaction mode of metal ions with purine derivatives – adenine and guanine, which are major constituents of DNA and RNA [16, 17].

The copper (II) complexes with ^{15}N – labeled lysine and ornithine produced at INCDTIM Cluj-Napoca were structural investigated in the third part by IR and EPR methods as powders, aqueous solution and adsorbed on NaY and HY zeolits.

The aminoacid complexes, particularly with copper (II), have received the attention because they proved to be useful antibacterial agents, nutritive supplies for humans and animals, and also as models for metalloproteins [18].

Also ^{15}N stable isotopes are used as ideal internal standards in isotopic tracers for nutrition investigations, to elucidate details of nitrogen metabolism in vivo and protein metabolism in different diseases [19,20].

Experimental and computational details used for the investigation of the studied biomedical compounds are given in the adequate our published papers shown at references.

1. Pharmaceutical compounds

1.1. Gastrointestinal and Antidepressive compounds

Metoclopramide is a gastrointestinal drug that is often used to combat the nausea that occurs in patients who are undergoing treatment with anticancer agents, the physical–chemical properties of this drug being extensively investigated [21].

The physical processes and chemical reactions of this drug involved in the biological processes are often very sensitive to the medium pH values and usually is present as the protonated molecular species (Figure 1.) in the human organism (pH = 2-8).

The conjugate acid–base forms of the metoclopramide drug were investigated by Raman spectroscopy in the solid state and in aqueous solutions and by SERS when the molecules are adsorbed on a colloidal nanoparticles [22].

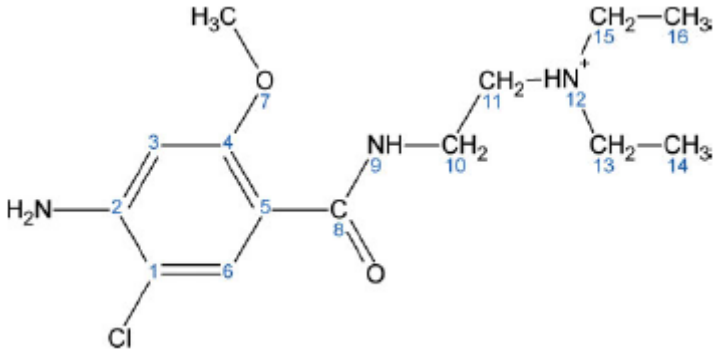

Fig. 1. Molecular structure of amine group protonated metoclopramide with atom numbering.

As shown in Figure 2 the protonated metoclopramide shows a different conformation of the diethylaminoethyl chain with respect to the unprotonated molecule. The new conformation of the protonated metoclopramide is favored by a supplementary hydrogen bond, which leads to a rotation of the diethylaminoethyl chain around the N9–C10 bond.

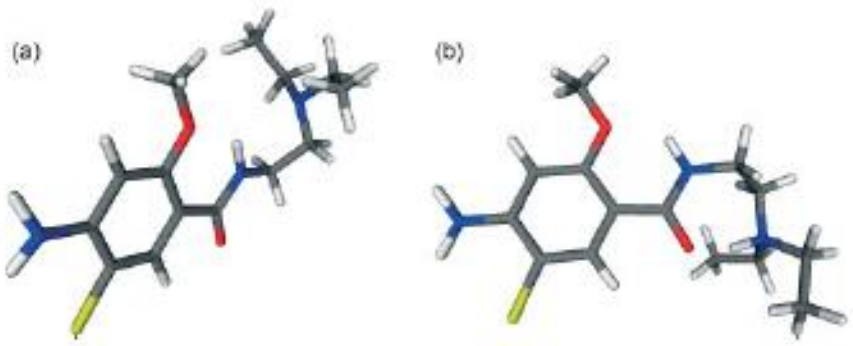

Fig. 2. Optimized geometries of the (a) neutral and
(b) the protonated metoclopramide molecular forms, at the B3LYP/6-31G(d) level of theory.

The C8N9C10C11 dihedral angle changes from −146.5° to 75.0° (calculated values) in perfect agreement with the experimental values corresponding to the unprotonated and protonated form, respectively (Table 1.[22]).

Also, the C10C11N12C13 dihedral angle changes from −78.6° of the unprotonated form to 149.9° for the protonated form leading to the formation of the N12H…OC8 intermolecular hydrogen bond, while the N9H … O7 hydrogen bond is preserved for both the unprotonated and protonated forms.

The calculated value (1.607 Å) of the length of this new bond N9H … O7 (1.607 Å) in the protonated metoclopramide form suggests the existence of a stronger hydrogen bond than in the unprotonated form.

Figure 3 presents the Raman spectra of metoclopramide aqueous solutions in the 3–8 pH range where the metoclopramide exists in the protonated molecular form.

The most evidenced Raman bands and their assignements are: 334 cm^{-1}- ip def(rg); 738 cm^{-1-} - breath(rg); 986 cm^{-1} - ν(C15C16); 1269 cm^{-1}- ν(N9C10), δ(C16H); 1315 cm^{-1} - ν(rg), δ(N2H); 1591 cm^{-1} - ν(rg), ν(C8O8), δ(N2H), δ(N9H), δ(N12H); 2999 cm^{-1} - ν(C10H) (Table 2. [22]). Abreviations used are: ip-*in-plane*, def-*deforming*, rg-*ring*, breath-*breathing*, ν-*stretching*, δ-*bending*.

The SERS spectra of metoclopramide in the 3–11 pH range can be divided in three parts (Figure 4.).

Firstly, at pH 3 only protonated metoclopramide molecules are adsorbed onto the silver nanoparticle surface.

Secondly, in the 6–8 pH range, on the silver nanoparticle surface both molecular species, protonated and neutral, coexist.

And thirdly, in the 9–11 pH range, only neutral molecules are adsorbed onto the silver surface.

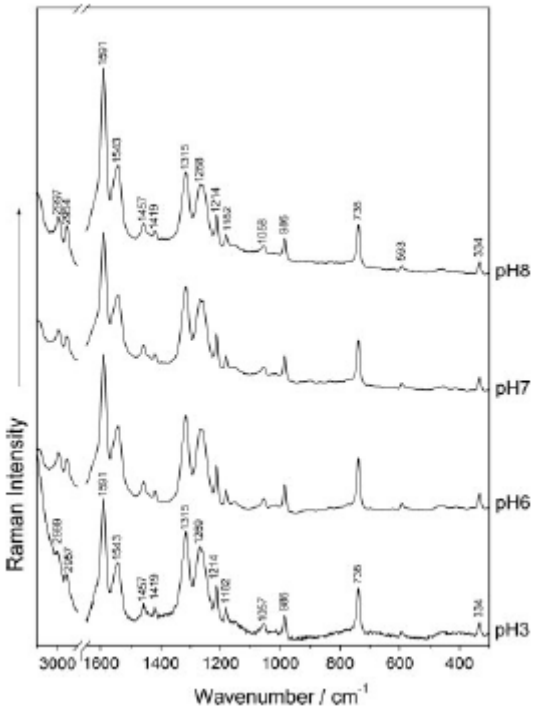

Fig. 3. Raman spectra of metoclopramide aqueous solutions in the 3-8 pH range.

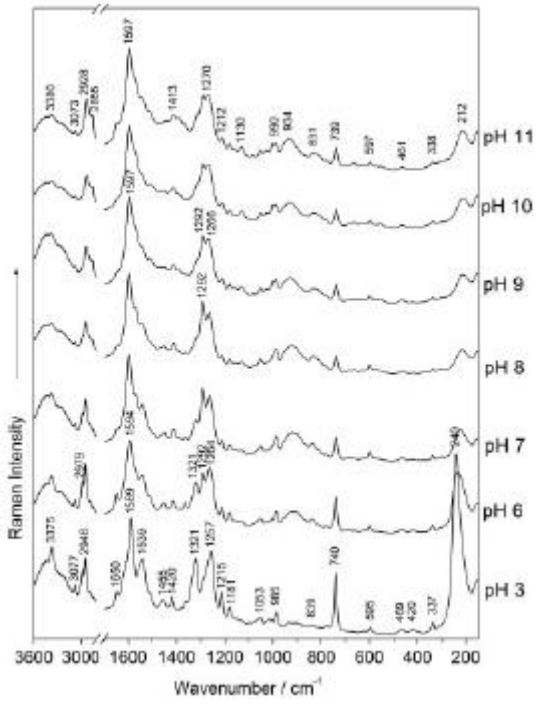

Fig. 4. SERS spectra of metoclopramide in the 3-11 pH range.

Marker bands in the SERS spectra at pH 3 and theirs assignements are: 1257 cm^{-1} - ν(C5C8), ν(N9H), δ(C10H), δ(C11H); 1321 cm^{-1} - ν(rg), δ(N2H); 1539 cm^{-1} - ν(rg), δ(N9H); 1589 cm^{-1} - ν(rg), ν(C8O8), δ(N2H), δ(N9H), δ(N12H) (Table 2 [22]).

At pH 3value, the metoclopramide–Ag stretching vibration (212 cm^{-1}) is overlapped by the intense band from 240 cm^{-1} due to the stretching vibration ν(Ag–Cl^-) of the Cl^- anions adsorbed on the silver surface. The metoclopramide–Ag stretching band (212 cm^{-1}) becomes evident in the SERS spectra recorded at basic pH values (over pH7).

The shape of the SERS spectrum at pH 6 is analogous to the pH 3 spectrum, indicating the presence of mainly protonated metoclopramide molecular species adsorbed on the silver surface.

Also at pH 6, a new peak appears at 1292 cm^{-1}, attributed to the neutral metoclopramide molecules, which is very intense in the SERS spectra at basic pH values. This peak assigned to the ring stretching vibration is characteristic to the neutral molecular species according to DFT calculations.

At pH 7 and 8, the presence of neutral molecular species adsorbed on the silver surface is more evident. The peaks from 740 cm^{-1}, 1321 cm^{-1} and 1539 cm^{-1} due to the protonated metoclopramide molecules, decrease furthermore in intensity, whereas the peak at 1292 cm^{-1} attributed to the neutral metoclopramide molecular species increases in intensity, revealing that the number of neutral molecules adsorbed on the silver surface has increased.

The presence of the intense bands at 1266 cm^{-1}, 1292 cm^{-1} and 1597 cm^{-1} suggest the adsorption exclusively of the neutral metoclopramide molecules on the silver surface, at pH values over 9. Also the peaks from 1321 cm^{-1} and 1539 cm^{-1} characteristic to protonated metoclopramide molecular species decrease in intensity and disappear totally in the SERS spectra at pH values over 9.

According to the SERS selection rules, and the changes in intensity of the ring-breating mode from 740 cm^{-1} with the increasing of pH values, we suppose that the protonated metoclopramide molecular species are adsorbed in a perpendicular orientation of the skeletal ring to the silver surface, whereas the neutral ones are adsorbed in a tilted orientation to the silver surface. At pH values over 6, the unprotonated N12 atom can be also involved in the tilted orientation adsorption process.

An other structural investigated compound is paroxetine (3S,4R)-3-

[(1,3-benzodioxol-5-yloxy)methyl]-4-(4-fluorophenyl) piperidine, used to treat major depression, obsessive–compulsive, panic, social anxiety, and generalized anxiety disorders in adult outpatients [23,24]. Its optimized structure by DFT calculation at B3LYP/6-31G(d) level of theory is shown in Figure 5.

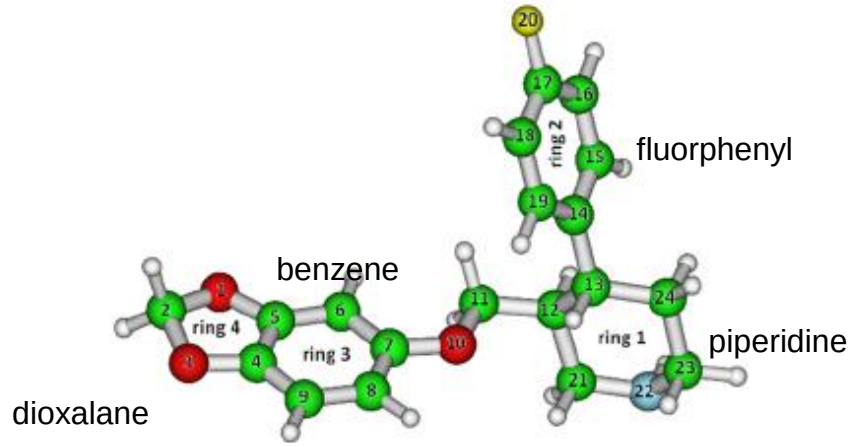

Fig. 5. B3LYP/6-31G(d) optimized geometry of paroxetine with the atom ring numbering scheme.

Experimental and calculated IR absorbance spectra of paroxetine in the 600–3500 cm^{-1} spectral range are shown in Figure. 6. The bands situated at 765 cm^{-1}, 914 cm^{-1} and 931 cm^{-1} are due to bending vibrations of the piperidine ring and of $C11H_2$ group, respectively. Bending vibrations of the ring3 are mainly contributing to the experimental bands at 781, 835, 944, 1097, 1183, 1247 and 1279 cm^{-1}, while normal modes corresponding to ring4 are associated with the experimental bands at 675 and 1381 cm^{-1}. Contributions from this ring are also seen in the normal modes assigned to the 781 and 944 cm^{-1} bands [25].

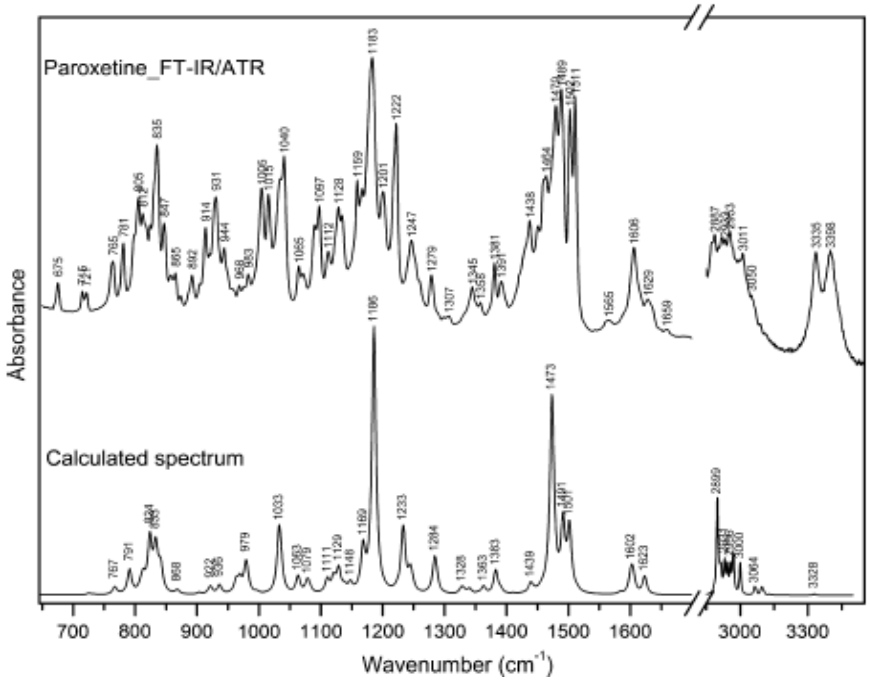

Fig. 6. Experimental FTIR (top) and calculated IR (botton) spectra of paroxetine.

The band located at 1040 cm^{-1} is also related to ring vibrations, being assigned to in plane deformations of $C2H_2O_2$ group from dioxolane ring (4) coupled with CC stretchings in ring1. The bands of 1381 cm^{-1} and 1438 cm^{-1} are due to the stretching vibration of CO group from dioxalane ring4.

Also the intense bands from 1222 cm^{-1} and 1502 cm^{-1} are characteristic to CF stretching vibration from fluorphenyl ring2.

The FT-Raman bands (Figure 7) from 253, 470 and 573 cm^{-1} are mainly due to the in plane deformations of piperidine ring(1) and benzene ring(2). The rocking vibrations of $C11H_2$ group superposed with out of plane deformations of ring3 appear at 351 cm^{-1}.

The breathing vibrations of benzene ring(2) and benzodioxol ring(3 and 4) appear at 846 and 805 cm^{-1}, respectively, giving rise to intense experimental bands.

The band from 1197 cm^{-1} is due to the stretching of the bond between piperidine and fluorophenyl rings coupled with in plane bending vibrations of CH groups from benzene ring(2).

Beside this band and that from 1218 cm^{-1} is also characteristic for the fluorophenyl ring.

The bending and stretching vibrations of the benzene ring contribute significantly to the normal modes giving rise to the Raman bands at 1297 cm^{-1} and 1604 cm^{-1}. The 1063 cm^{-1}, 1094 cm^{-1}, 1159 cm^{-1} and 1502 cm^{-1} bands are associated with vibrations characteristic for the dioxolane ring.

SERS spectra of paroxetine (Figure 7), due to the interactions of this molecule with the silver nanoparticles surface are characterized by an intense band at 243 cm^{-1} due to Ag–O [26] or Ag–N [27,28] bonds vibrations.

Our calculation for the wavenumbers of these two bonds shown 244 cm^{-1} for Ag–N(22) and 226 cm^{-1} for Ag–O(10) [25].

The intense SERS band at 812 cm^{-1} is due to the breathing vibration of the benzodioxol ring(3+4) adsorbed in a tilted orientation, in the near vicinity of the silver surface. The SERS band from 1605 cm^{-1}, assigned to CC stretching and to in plane bending vibrations of CH groups from benzene ring(3), supports also this hypothesis.

The perpendicular orientation to the silver surface of piperidine ring(1) is proved also by the enhanced SERS bands from 966 cm^{-1} to 988 cm^{-1} region due to CC stretching vibrations of this ring. The intense SERS bands at 1363cm^{-1} and 1452cm^{-1}, due to the in plane bending vibrations of CH_2, CH and NH groups from piperidine ring, are further proofs for its perpendicular orientation on the silver surface.

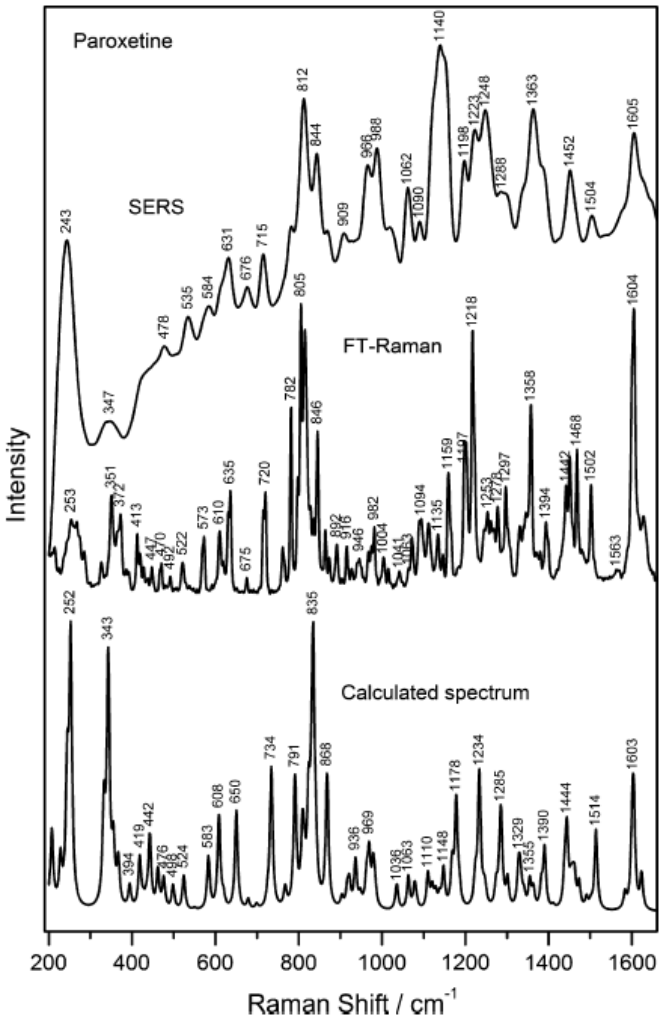

Fig. 7. SERS, FT-Raman and calculated Raman spectra of paroxetine.

These data and the SERS selection rules show that the adsorption of paroxetine to silver nanoparticles occurs through the oxygen (1,3,10) and nitrogen (22) atoms.

The benzodioxol ring is adsorbed in a tilted orientation, in the near vicinity of the silver surface, while the piperidine ring and benzene ring(2) are perpendicular oriented on the silver surface.

1.2. Angina pectoris and cardiovascular drugs

Amlodipine (3-ethyl-5-methyl-2-(2-aminoethoxymethyl)-4-(2-chlorophenyl)-1,4-dihydro-6-methyl-3,5-pyridinedicarboxylate) is used to treat high blood pressure and chest pain (angina), being one of the most widely prescribed cardiovascular drugs [29].

In practice it is administered with the addition salts in order to improving its solubility, stability, non-hydroscopicity and processability [29, 30]. Thas the amlodipine besylate (AM) salt fulfils all these requirements (Figure 8.).

Latosinka and coworkers performed ^{13}C NMR and ^{35}Cl-NQR studies on amlodipine besylate [31, 32] and concluded that no substantial molecular structure differences exist between the solution and solid state of AM.

Asymmetric stretch of amine group gives rise to the band at 3300 cm^{-1} in the FT-IR spectrum (Figure 9.) with the corresponding calculated wave number of 3376 cm^{-1}.

The symmetric stretch of the same group is seen as a week band in the Raman spectrum at 2800 cm^{-1} with the calculated wave number (2804 cm^{-1}) in perfect agreement with the experiment and with a previously study reported by Rollinger and Burger [33].

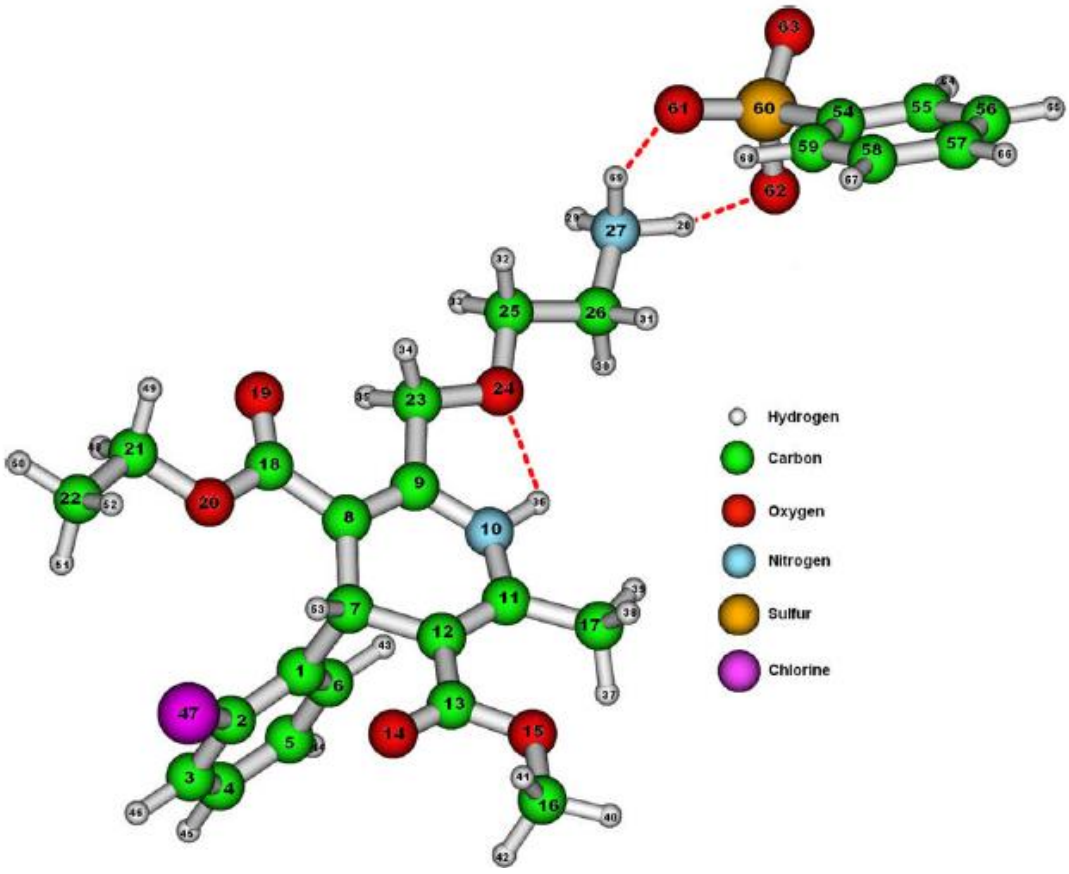

Fig. 8. Optimized molecular structure corresponding to the lowest energy conformer and atom numbering of amlodipine besylate.

Another characteristic band due to the asymmetric deformation of NH_3^+ calculated at 1623 cm^{-1} is seen as a strong band at 1616 cm^{-1} in the FT-IR spectrum and 1615 cm^{-1} in Raman.

This fact is supported by the study of Foley and Enescu [34] who observed this mode ($\delta_{as}(NH_3^+)$) at 1614 cm^{-1} for cysteine zwitterions.

Umbrella-like vibration of NH_3^+ has a calculated wave number of 1391 cm^{-1} and it corresponds to the bands seen at 1384 and 1382 cm^{-1} in the FT-IR and Raman spectra, respectively.

A predominant wagging mode for the same group is predicted at 1265 cm^{-1} in perfect agreement with the experimental FT-IR band from 1265 cm^{-1}.

The very good agreement between the experimental and the calculated vibrational IR and Raman bands wavenumbers of amlodipine besylate as well as the identification of the main characteristic group frequencies (Table 1. [35]) correspond to the optimized structure (Figure 8.).

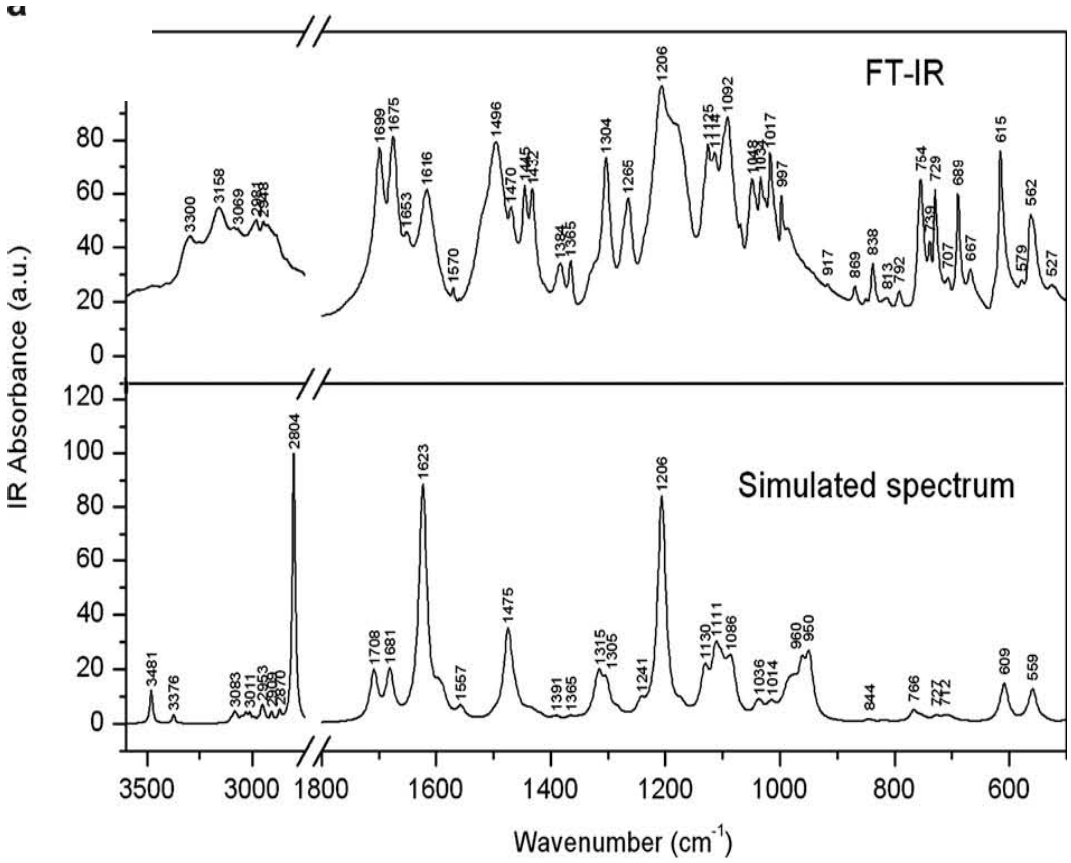

Fig. 9. Experimental and simulated FT-IR spectra of amlodipine besylate.

The best performance in reproducing the ^1H NMR spectrum of amlodipine in liquid state samples using DMSO-d_6 as deuterated solvent and DFT computed chemical shifts (Table 2. [35]) suggests the presence of hydrogen-bonded protons. The chemical shift of amine protons ($N(27)H_3$) is very well reproduced by B3LYP/6-31G(d) method (7.86 ppm experimental and 7.69 ppm calculated). The calculated 3D electrostatic potential contour map of amlodipine besylate at the B3LYP/6-31G(d) level of theory predict the reactive electrophilic and nucleophilic attack sites as well as hydrogen bonding interactions of the investigated molecule.

The most negative V(r) value is associated with O(14), O(15), O(19), O(20), O(61), O(62) and O(63) with a value around –0.124 a.u., while the most positive value correspond to the NH_3^+ group (about 0.15 a.u.) and to $C(26)H_2$ and $C(25)H_2$ methylene groups (about 0.08 a.u.).

Other two compounds with large implications in medicine, the antiarrhythmic effects, the treatment of hypertension and angina pectoris [36,37], are pindolol (PIN) and verapamil (VER) molecules (Figure 10.).

The conformation of pindolol structure is well confirmed by our DFT calculations of some bond lengths and dihedral angles [38]. A very satisfying agreement is obtained between such calculated (this work)/experimental pair parameters: C2-N5 = 1.379/1.373 Å, C9-N5 = 1.385/1.366 Å, C3-O8 = 1.367/1.368 Å, C11-O8 = 1.417/1.434 Å, C12-O4 = 1.428/1.422 Å, C13-N15 = 1.455/1.460 Å, C16-N15 = 1.467/ 1.485 Å, O8 … O14 = 2.841/2.839 Å, N15-O14 = 2.839/2.820 Å.

The calculated/experimental values for valence and dihedral angles defining hydrogen bonding parameters are: C12O14H30 = 117.6/107.7^0, C13N15H31 = 103.5/106.8^0, C12C13N15H31 = -45.3/-44.1^0.

The 759 cm^{-1} band from FT-IR spectrum of pindolol (Figure 11.) is due to the out of plane bending vibration characteristic of O14H group. The band from 883 cm^{-1} is due to the superposition of the out of plane deformation vibrations of N15H group with the in plane deformations of aliphatic carbon (C11C12C13) chain. The stretching vibration of C11O8 group and in plane bending vibration of CH groups appears at 1047 cm^{-1}.

The superposition of the in plane vibrations of the ring NH and CH groups, and also of C5-O10 group with NH, CH groups, are situated at 1246 cm^{-1} and 1286 cm^{-1} respectively. The in plane deformations of CCC and CNC groups from benzene and pyrolline rings are superposed at 1366 cm^{-1}. Another intense superposition of in plane bending vibrations of N5H and $C11H_2$ groups appear at 1519 cm^{-1}. At high wavenumbers 2838 cm^{-1}, 2966 cm^{-1} and 3308 cm^{-1} the stretching vibrations of $C13H_2$, CH aliphatic and N15H groups appear, too. Similar assignments were also done for IR spectra of verapamil.

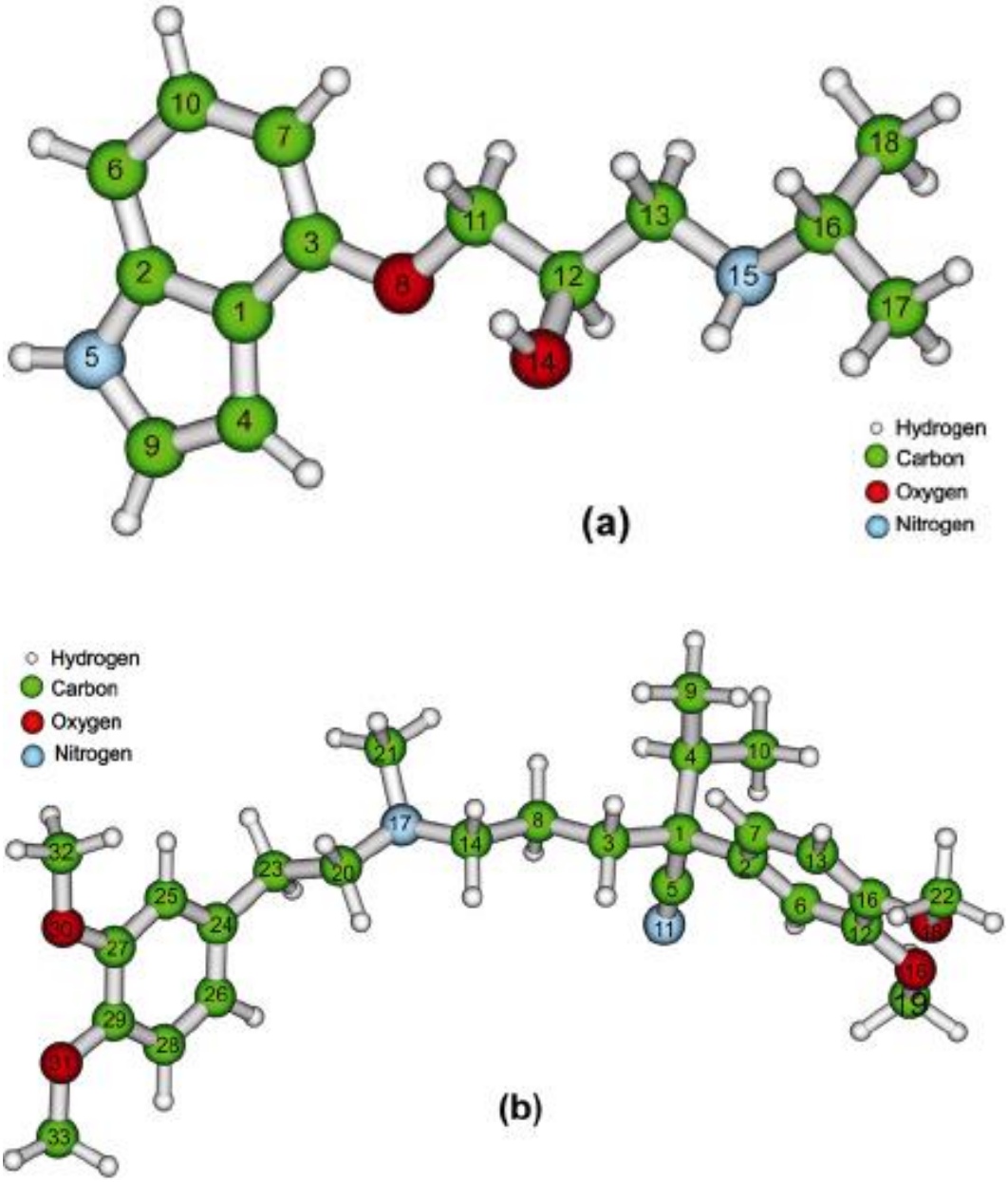

Fig. 10. B3LYP/6-31(d) optimized molecular structures of pindolol (a) and verapamil (b).

Some minor modifications in band positions and intensities were observed between Raman and SERS spectra of pindolol [38].

Theoretically, the interaction of PIN with the silver surface can be established through the lone electron pairs of the oxygen and nitrogen atoms of PIN or through the π electrons of the rings.

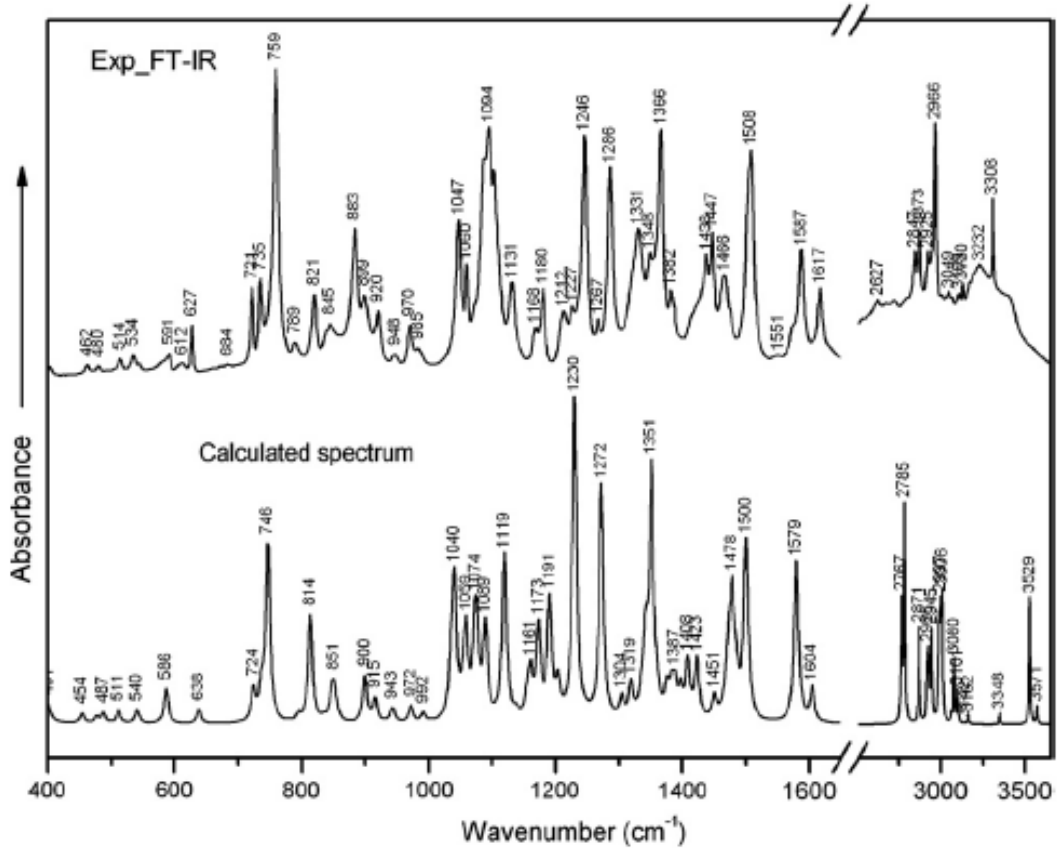

Fig. 11. Experimental FT-IR and calculated IR spectra of PIN.

The MEP distribution [38] of the PIN molecule obtained from DFT calculations shows that, the negative charge is located mainly on the oxygen (O8, O14) and the nitrogen (N5, N15) atoms.

Thus, the adsorption of the PIN molecule to the silver surface is supposed to occurred through these oxygen and nitrogen atoms and also through the π electrons of the rings in a flat orientation.

Raman and SERS spectra of verapamil (Figure 12.) and the characteristic bands of the investigated molecules were also analyzed.

A weak band at 267 cm^{-1} due to the rocking vibrations of CH_3 groups can be observed in the FT-Raman spectrum of verapamil.

The band from 385 cm^{-1} is due to the bending vibrations of CH_2, CH_3 groups bonded to the O16, O18, O30 and O31 atoms. The C-C stretching vibrations of ring1 superimposed with its CH deformation vibrations are localized at 769 cm^{-1}, 1035 cm^{-1} and 1519 cm^{-1}. Similar vibrations for ring2 appear at 1606 cm^{-1}.

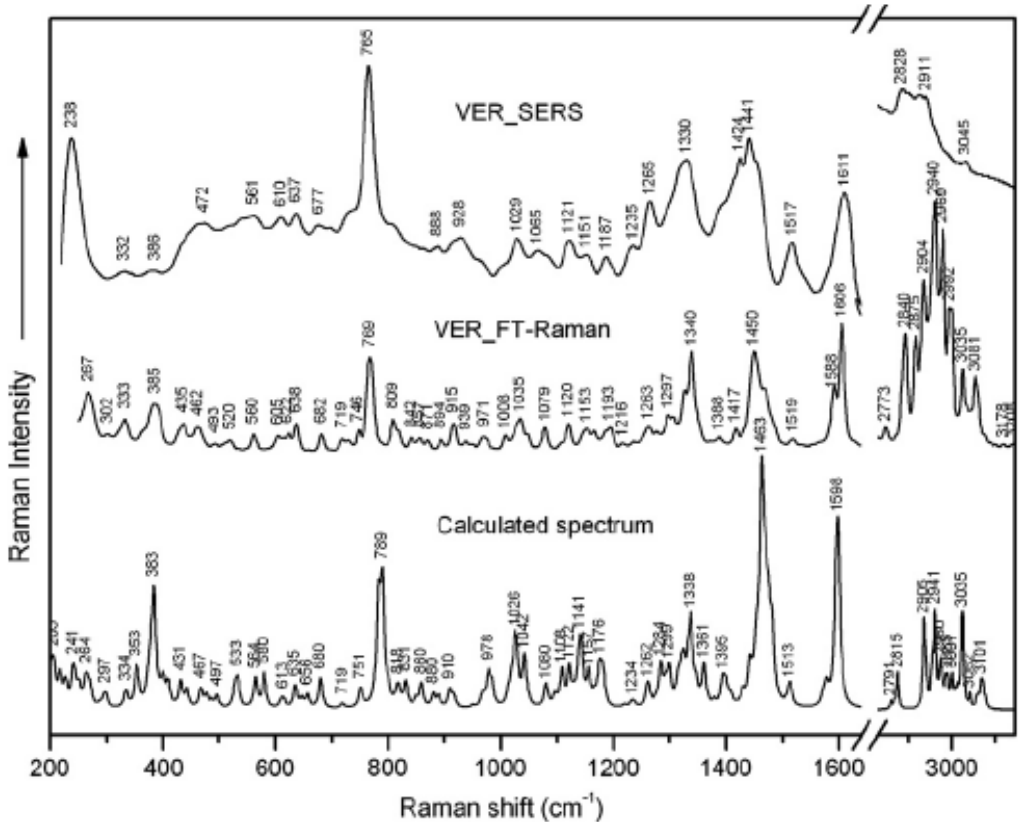

Fig. 12. SERS, FT-Raman and calculated Raman spectra of VER.

A superposition of bending and rocking vibrations of CH_2 groups are situated at 1340 cm^{-1}. Also, the superposition of bending vibrations of CH_2 and CH_3 groups is at 1450 cm^{-1}. The bands from 2940 and 3035 cm^{-1} are due to the symmetric and asymmetric stretching vibrations of some CH_3 groups.

The bands 769, 1035, 1340, 1450, 1519 cm^{-1} from Raman spectrum, due to the stretching C-C rings vibrations and deformation vibrations of CH_2, CH_3 groups, increase in intensity in the SERS spectrum of verapamil and are shifted to lower wavenumbers (Figure 12.). An intense band at 238 cm^{-1} due to the Ag-O bond formation appears also in the SERS spectrum of VER due to a strong interaction of its oxygen atoms (O16, O18 and O30, O31), bonded to the benzene rings, with the silver nanoparticles surface.

Taking into account the SERS surface selection rules [39,40] and the MEP of VER which shows that the negative charge is located mainly on the four oxygen atoms (16, 18, 30, 31) we can finally conclude that the VER molecule adopts a bent conformation on the silver surface, strongly fixed by the oxygen atoms and a perpendicular orientation of the benzene rings to the silver surface.

Atenolol (4-[20-hydroxy-30-[(1-methythyl)amino]propoxy]-benzeneacetamide – ATE) and metoprolol (1-(isopropylamino)-3-[p-(2-methoxyethyl)phenoxy]-2-propanol – MET), shown in Figure 13., are widely prescribed in medicine as cardioselective β_1-adrenergic blockers [41,42].

Since different conformations or enantiomers of such molecules can drastically influence their physico-chemical behavior and pharmacological activity, the knowledge of their structures is of great importance.

The assignment of the all vibrational bands is accomplished by DFT calculations at B3LYP/6-31G(d) level of theory.

Previously reported studies on vibrational properties of ATE are focused particularly on hydrogen bonding interactions [43] and the interaction between ATE and β-cyclodextrins [44].

X-ray structure of the MET compound shown that it crystallizes in an N-protonated form, being hydrogen bonded to two succinate anions [45].

The ATE molecule has a chiral center giving rise to (R) and (S) enantiomers (Figure 13.a).

The S-ATE conformer has the amino group rotated in a such a way that one of its NH bond is involved in a π hydrogen bonds (HB) interaction with the phenyl group of the molecule, a situation that does not occur for the (R,S) conformer.

For MET compound we optimized the protonated and unprotonated forms [46], as well as the molecular complex formed between the N-protonated MET cation and two hydrogen bonded succinate anions (Figure 13.b) using as starting geometries the experimental structures [45].

The main difference between the HB and non-HB MET is a slightly different orientation of the two terminal CH_3 group relative to the neighbor amino group, as well as a change in the lengths of the $H_2C–NH_2$ and $H_2N–CH$ bonds.

Thus, in the non-HB conformer, the two bond lengths are 1.510 and 1.531 Å, while for the MET-2 succinate complex they are significantly shorter (1.494 and 1.508 Å).

The experimental and the calculated IR and Raman spectra of the (S)- and (R,S)-ATE conformers in band positions and their intensities are given in Table 1.

It can be seen that the Q4, Q8, Q9, Q12, Q14 and Q21 modes are predicted almost equally well by both (S) and (R,S) conformers.

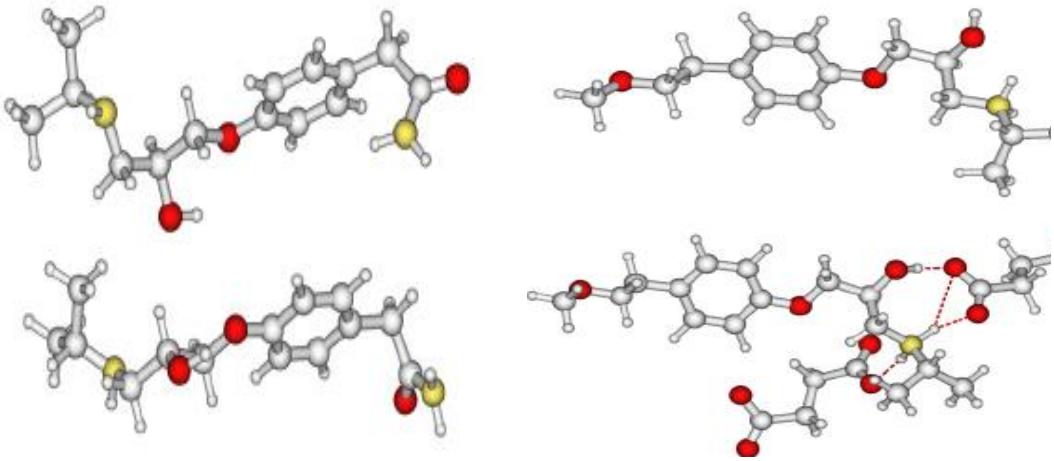

Fig. 13. B3LYP/6-31G(d) optimized geometries of (S)-atenolol, (R,S)-atenolol (a) and metoprolol, complex metoprolol-2 succinate anions (b).

Table 1. Experimental and B3LYP/6-31G(d) calculated vibrational spectra of atenolol

Mode	Experimental		Calculated*				Assignments
			(S)-ATE		(RS)-ATE		
	FT-IR/ATR	Raman	IR	Raman	IR	Raman	
Q1			3588 vw		3586 vw	3586 w	ν(OH)
Q2	3356 s		3574 w	3574 vw	3554 vw	3554 w	$\nu_a(NH_2)$
Q3	3174m		3453 vw	3453 m	3437 vw	3437 m	$\nu_s(NH_2)$
Q4		3070 s		3089 m	3052 vw	3087 s	ν(CH ring)
Q5	2965 w	2969 s	2990 w		3007 vw	3007 s	$\nu_a(CH_3)$
Q6	2924 w	2915 vs		2923 vs	2952 vw	2933vs	$\nu_s(CH_3)$
Q7	1670 sh	1681 w					ν(CO)
Q8	1637 vs		1736 vs	1736 vw	1736 vs	1736 vw	ν(CO)
Q9	1612 w	1612 s	1607 w	1608 s	1607 w	1607 s	ν(CC ring)
Q10			1571 s	1570 s	1587 s		$\delta(NH_2)$
Q11	1583 vw	1583 w	1567 vw	1567 vw			ν(CC ring)
Q12	1517 m		1504 m		1503 m		ν(CC ring) + δ(CH ring) + $\delta(CH_2)$
Q13		1450 m		1449 w	1475 w	1461 w	$\delta(CH_3)$
Q14	1418 w	1421 w	1408 vw		1407 vw		δ(COH) + $\omega(CH_2)$
Q15	1302 vw	1301 m	1310 w	1312 vw	1334 m		$\delta(OCNH_2)$ + δ(CCC ring)
Q16	1243 m	1243 w	1245 s	1277 w	1244 vs	1267 vw	$\omega(CH_2)$
Q17		1205 s	1229 m	1228 vw	1226 m	1226 vw	δ(CH) + δ(OH) + δ(CCC ring)
Q18	1180 vw	1183 m		1186 vw			ν(CC) + δ(CCC ring) + $\omega(CH_2)$
Q19		1141 m	1158 w	1166 vw	1135 vw	1149 vw	ν(HC–NH) + $\rho(CH_3)$
Q20	1038 vw	1038 vw	1025 w		1030 w		ν(C–O) + $\rho(CH_3)$ + δ(CH ring)
Q21	886 vw	886 m	888 vw	887 vw		888 w	ring breathing
Q22		859 vs		869 vw		865 vw	δ(CCC ring)
Q23	829 vw	829 m		826 vw	817 vw	836 vw	δ(CCC ring) + $\rho(NH_2)$
Q24	712 vw	722 m	749 vw	749 vw	759 vw	759 vw	δ(NH)
Q25		638 m		653 vw			δ(CCC ring) + $\tau(NH_2)$
Q26	568 vw	568 vw	558 vw		597 w		τ(ring) + δ(OC–NH_2)
Q27	427 vw		429 vw		430 vw		δ(OH)
Q28		368 vs	256 vs	362 vw	372 vs	345 vw	$\omega(NH_2)$

vs – very strong, s – strong, m – medium, w – weak, vw – very weak, sh – shoulder.

* scaled wavenumbers according to the procedure proposed by Scott and Radom [47].

The Q11, Q18 and Q25 modes are predicted only by the (S) conformer, while for Q13, Q15, Q24, Q26 and Q28 the same conformer predicts better band positions and/or intensities when compared to the (R,S) conformer. Both conformers predict Q17 and Q22 modes well their position but, much weaker than their experimental counterparts.

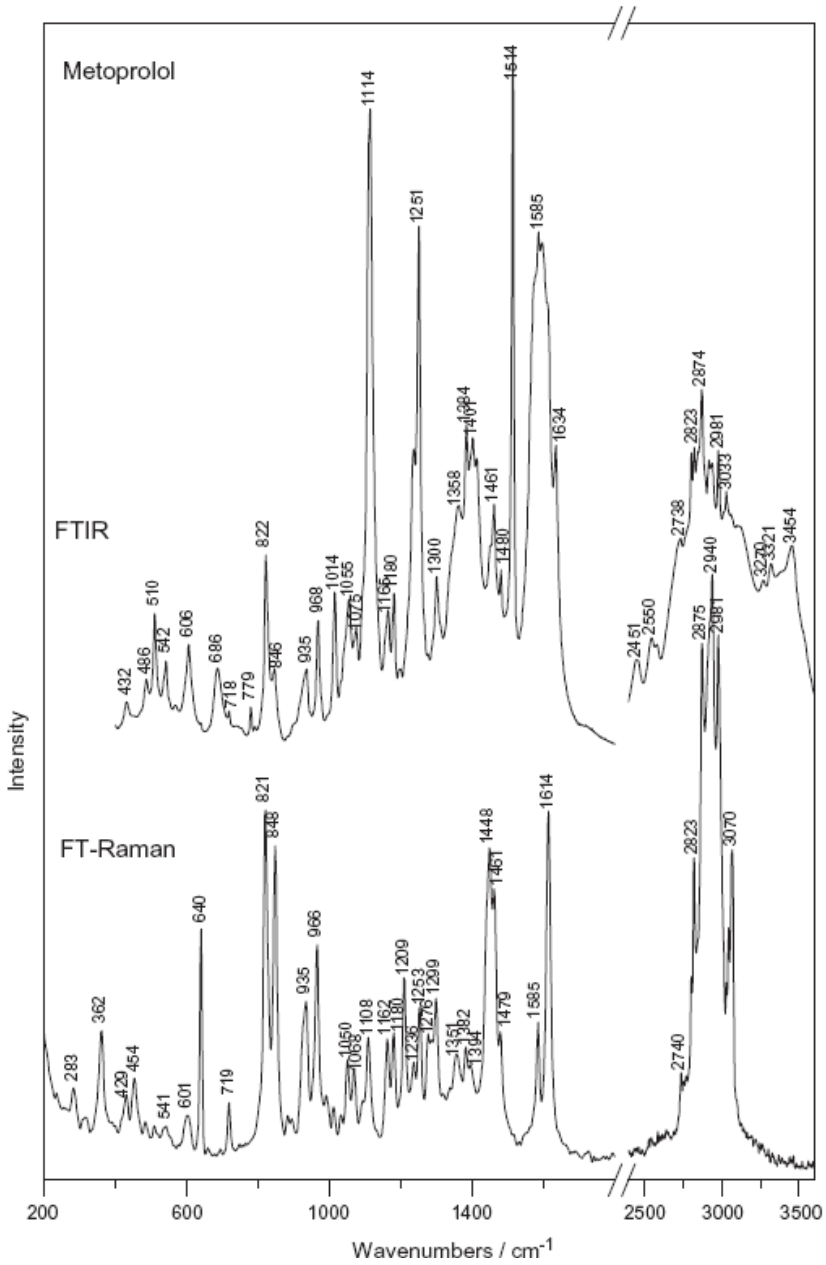

Fig. 14. FT-IR/ATR (top) and FT-Raman (bottom) spectra of metoprolol.

The major difference between the vibrational spectra given by the two structures of MET, N-protonated (MET^+) and also for MET^+-2 succinate anions complex (MET^+-2 SA^{2-}) are seen in the high wavenumber region (Figure 14.). Thus, the Q1–Q3 (ν(OH) and ν_{as}, ν_s (NH_2)H bonded) modes of MET^+-2 SA^{2-} are, as expected, reproduced at significantly lower wavenumbers than in the case of non-H bonded MET^+ (Table 2. [46]).

Similar behaviour is also observed for the Q_{11} mode at 1634 cm^{-1} corresponding to the δ(NH_2) group where the calculated bands for MET^+-2 SA^{2-} complex, are from 1593 to 1639 cm^{-1} due to the superposition of $\nu_{as}(CO_2)$ vibrations.

Two strong bands from the IR spectrum at 1251 cm^{-1} (Q_{22}) - δ(OH) and 1114 cm^{-1} (Q_{27}) - ν(CO) have the weak correspondent bands in the Raman spectrum.

Their wavenumbers and their intensities are excellently reproduced by DFT calculations, both for MET^+ and MET^+-2 SA^{2-} structures (Table 2. [46]).

Other two strong bands appear in the Raman spectrum at 848 and 821 cm^{-1}, assigned to ring breathing and to out of plane CH ring vibrations, respectively.

Because the solution used for the SERS measurements has pH = 8.5, in order to discuss the SERS spectra we will consider the protonated forms of ATE and MET molecules.

Comparing the Raman and SERS spectra of atenolol we have concluded that ATE molecules adsorb to the silver surface with the phenyl ring and the methyl-amino-propoxy chain in a tilted orientation relative to the silver surface.

The bent conformation of MET allows a more parallel alignment, flat orientation, of the aromatic ring while the two ends of the molecule are pointing away from the silver surface.

Besides showing an enhanced pharmacological activity, metal complexes of different drugs exhibit a variety of new pharmacological effects such as antiulcer, anti-diabetic, anticancer, anticonvulsant and radiation recovery activities [48]. For a better understanding of their activity, such complexes are structurally investigated by FT-IR and EPR spectroscopic methods [49].

The strong IR band at 3356 cm^{-1} assigned to the NH_2 group of atenolol, is shifted to 3452 cm^{-1} after the complexation with copper (Figure 15.).

Also, the very strong ν(C=O) band at 1637 cm^{-1} in the IR spectrum of ATE is shifted to 1655 cm^{-1} in the spectrum of the Cu–ATE complex, showing the involvement of this oxygen atom in the coordination. The ν_s band of the NH_2 group found at 3174 cm^{-1} in the spectrum of ATE shifts at a higher wavenumber (3375 cm^{-1}), suggesting the cleavage of hydrogen bonds during the complexation.

The band corresponding to the δ(OC–NH_2) vibration is red-shifted from 568 cm^{-1} in the free ligand to 514 cm^{-1} in the complex. Also, a new band appears in the spectrum of the complex at 459 cm^{-1} confirming again the complexation of the Cu(II) ion by the ATE ligands, through the carbonyl group. The bands from 1299 cm^{-1} and 1235 cm^{-1} assigned to δ(OH) and ν(CO) are drastically reduced in intensity in the spectrum of Cu-MET complex.

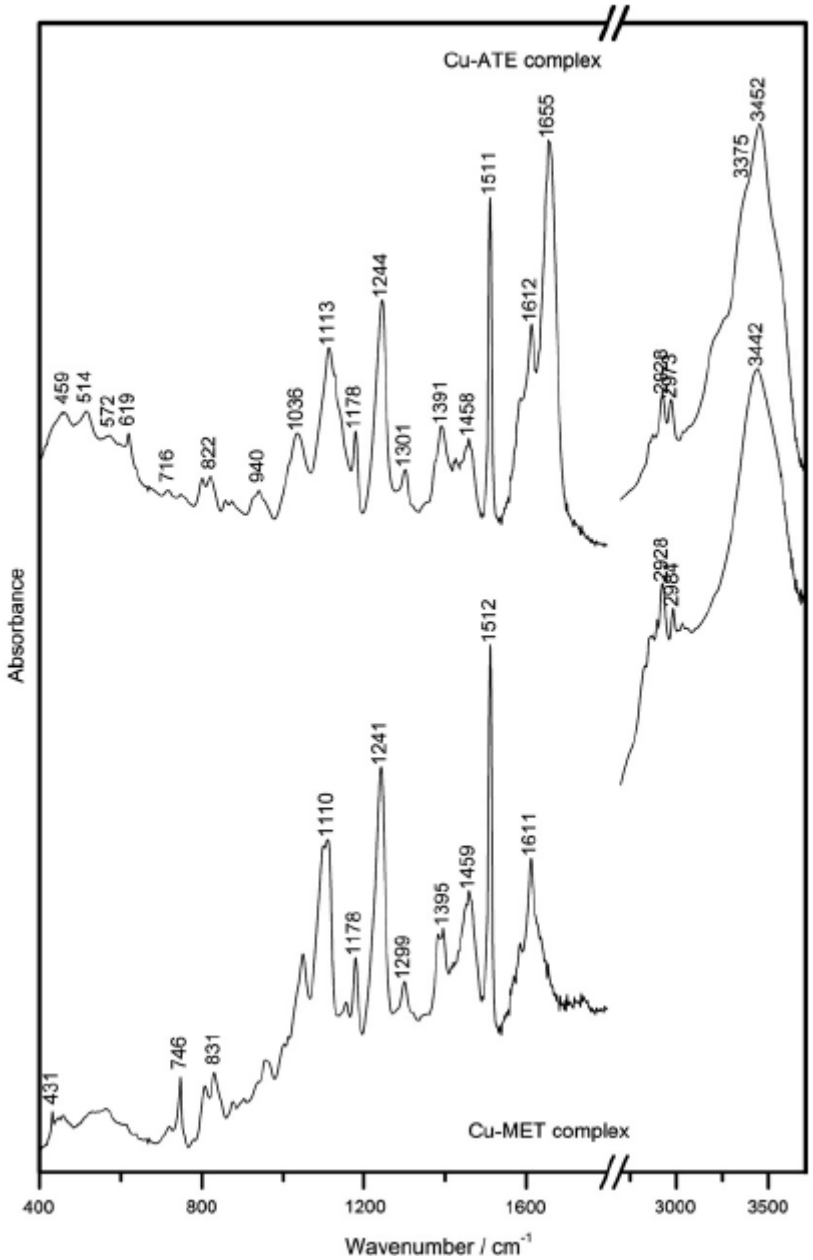

Fig. 15. FT-IR spectra of Cu(II)–ATE (top) and Cu(II)–MET (bottom) molecular complexes.

The broad bands at 1611 and 1459 cm^{-1} in the spectrum of the complex are assigned, according to Padmanabhan et al. [50], to ν_{as} and $\nu_s(CO_2^-)$ vibrations of the succinate anions bonded to the Cu(II) ion.

According to the DFT calculations performed on the succinate anion itself, the new band that appears in the spectrum of the Cu–MET complex at 746 cm^{-1} is assigned to a $\delta(OCO) + \delta(CCC)$ vibrational mode of the succinate anion.

Raman spectrum of the complex (not shown here) exhibits also two bands at 236 cm^{-1} and 204 cm^{-1} which are also assigned to Cu–O vibrations with the oxygen atoms from the succinate anions. Thus, the present data show that Cu(II) ion in MET complex is coordinated by oxygen atoms from the succinate anions.

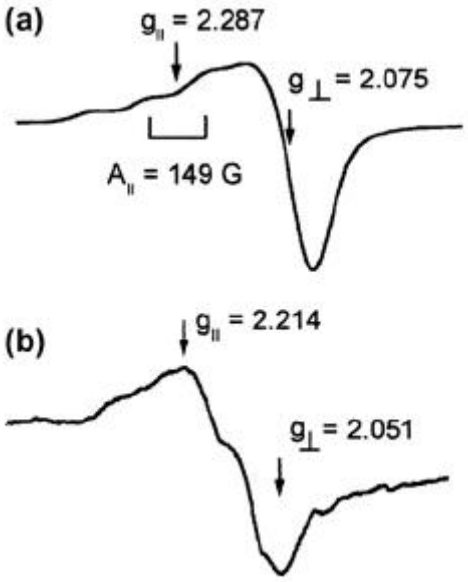

Fig. 16. EPR spectra of Cu(II)–ATE (a) and MET (b) complexes.

Powder EPR spectra of the Cu(II)-complexes obtained at room temperature (Figure 16.) exhibit the absorption signals typical for randomly oriented single state (S = 1/2) species with axial symmetry and $d_{x^2-y^2}$ orbital as ground state for the paramagnetic electron in the Cu–ATE complex [51]. Comparing the shape of the spectrum and the values of characteristic EPR parameters ($A_{\|}$, $g_{\|}$, $g_{\perp}$) of Cu(II)–ATE complex with those obtained for other Cu(II) complexes with nitrogen and oxygen ligands, allows us to conclude that the local symmetry around the metal ions is of square-planar type with a CuN_2O_2 chromophore in the xOy plane [52]. Such a chromophore is possible as a result of the coordination of two ATE molecules, each of them being bonded to the Cu(II) ion through the oxygen and nitrogen atoms in the amide groups [53].

The spectrum of Cu(II)–MET complex suggests the presence of two monomeric species, one of them with $d_{x^2-y^2}$ ground state (having $g_{\|} > g_{\perp}$) and the other one with d_{z^2} ground state (characterized by $g_{\perp} > g_{\|} = 2.0023$) [54]. The last species is a very rare case of local symmetry which suggests the existence of strong Cu–O bonds in the case of Cu(II)–MET compound, most probably due to the coordination of the succinate anions by the Cu(II) ion.

1.3. Compounds with antibacterial potential

Development of novel therapeutics for the treatment of microbial infections has become a clinical imperative. From this perspective, oxazolidinones have attracted great attention as a new class of active synthetic antibiotics with mechanism of bacterial protein synthesis inhibition [55,56].

For these reasons we become interested in the molecular and electronic structure of 5-para-nitro-benzylidene-thiazolidine-2-thione-4-ones (5pN-BTT) as potent antimicrobial agents synthesized at the Iuliu Hatieganu University of Medicine and Pharmacy and the preliminary results proving a superior antibiotic activity than the ampicilin used as reference [57].

The molecular structure of 5pN-BTT with one THF (tetrahydrofuran) solvent molecule (Figure 17.) determined by single-crystal X-ray diffraction measurements have been deposited with the Cambridge Crystallographic Data Centre as Supplementary Publication CCDC-No703556.

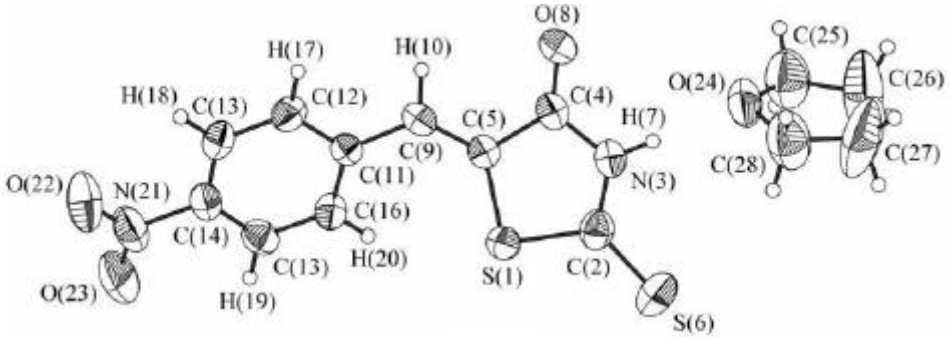

Fig. 17. ORTEP diagram of 5pN-BTT · THF structure.

This crystallizes in the monoclinic space group C2/c with Z = 8 and cell parameters a = 29.496(9) Å, b = 7.276(2) Å, c = 14.873(4) Å, $\alpha = 90.0^0$, $\beta = 95.161(6)^0$ and $\gamma = 90.0^0$ [57].

Hydrogen bond length O(24)...H(7) realized between 5pN-BTT and THF molecules is of 1.90(5)Å. 5pN-BTT molecules form a polymeric chain due to the intermolecular O(8)…H(19) (2.61 Å) hydrogen bond between pairs of molecules

and each 5pN-BTT molecule is also linked to a solvent molecule through the above mentioned O(24)…H(7) hydrogen bond, along the crystallographic *c* axis.

There are three possible tautomeric forms (thione, thiol and enol) in gaz-phase and in water and DMSO solutions of this compounds (Figure 18.).

According to the DFT calculations at B3LYP/6-31G(d) level of theory we found that the lowest energy tautomer is in thionic form.

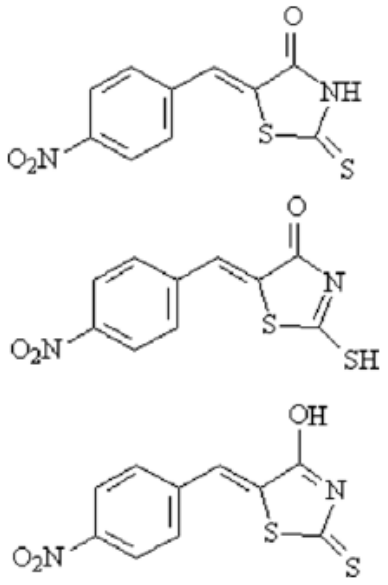

Fig. 18. Thione, thiol and enol tautomers of 5pN-BTT molecule.

The thione–thiol tautomeric equilibrium has a significant importance in biochemistry. In liquid phase, the two tautomeric forms (thione and thiol) can convert into each other by a direct proton transfer mechanism. However, a solvent assisted proton transfer reaction is also plausible due to the fact that NH donor and C=S acceptor H bonding sites are available for stable complexes formation which are predicted to greatly decrease the energy barrier height [58].

For 5pN-BTT molecule, the C(2)-N(3) bond length decreases from 1.362 to 1.280 Å, while the N(3)-C(4) and C(2)-S(6) distances increases from 1.382 and 1.644 Å to 1.413 and 1.751 Å, respectively, in going from thione to thiol form.

The ^{1}H NMR measurements on the investigated compound 5pN-BTT were made on liquid state samples, using DMSO-d_6 as deuterated solvent and the corresponding experimental spectra are given in Figure 19.

The peak at 7.74 ppm is assigned to the H(10) proton, while the two doublets centered at 8.34 and 7.86 ppm are assigned to the two pairs of protons H(18)-H(19) and H(17)-H(20), respectively.

For elucidated this fact we calculated the NMR spectrum of the 5pN-BTT·2DMSO complex, obtained by placing two DMSO near the NH group of the 5pN-BTT molecule. The chemical shift at 14.05 ppm in the 1H NMR spectrum of 5pN-BTT is assigned to the hydrogen-bonded proton of the thione conformer, while the signal at 3.37 ppm is assigned to the proton bound to S(6) atom in the thiol conformer [59].

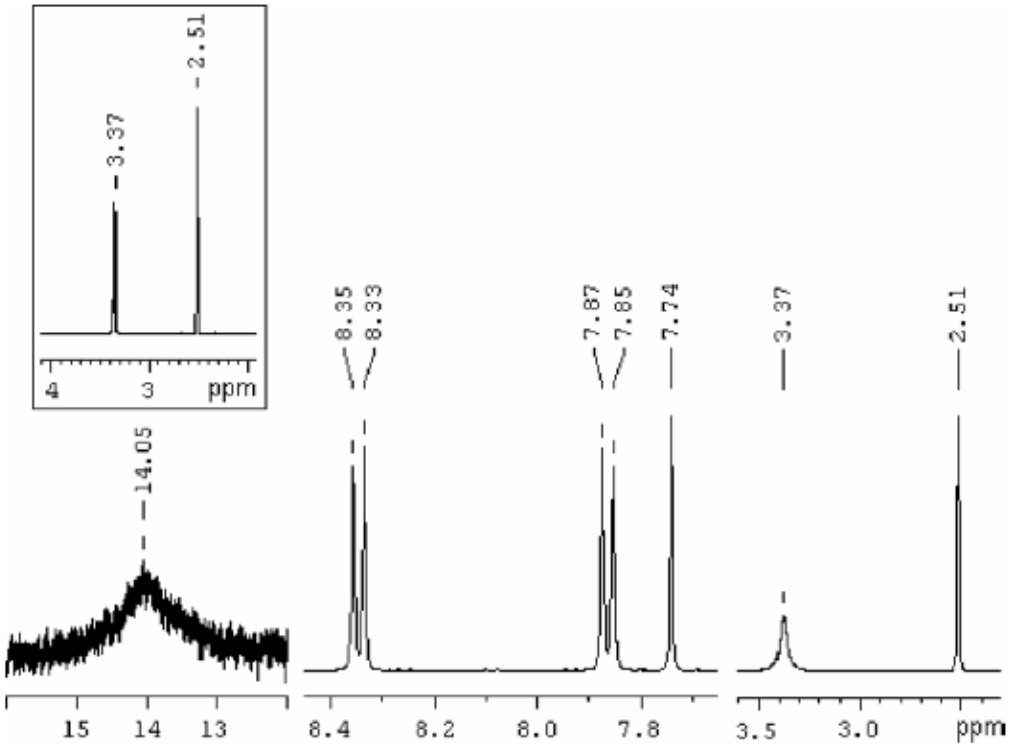

Fig. 19. 1H NMR spectrum of 5pN-BTT molecule; inset: 1H NMR spectrum of DMSO solvent.

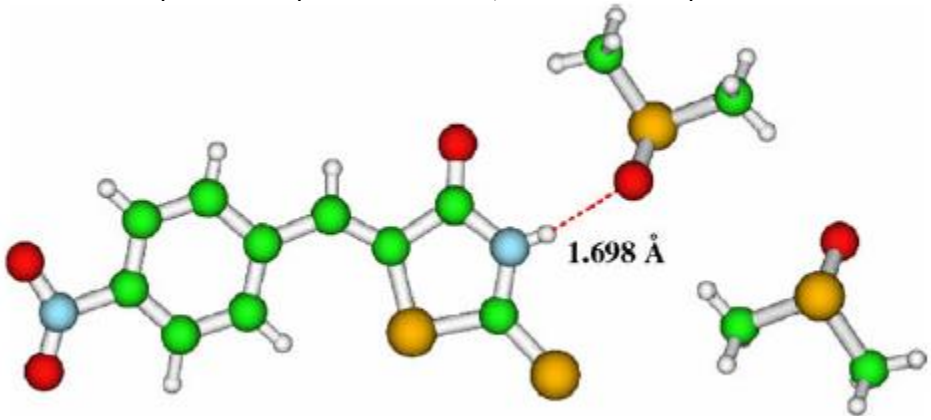

Fig. 20. Optimized geometry of 5pN-BTT · DMSO complex, calculated at B3LYP/6-31G(d,p) level theory.

Theoretical chemical shift for hydrogen-bonded H(7) proton is 14.35 ppm, in very good agreement with experiment. On the other hand, the SH proton in the thiolic tautomer has a calculated chemical shift of 4.12 ppm, in satisfactory agreement with the experimental value of 3.37 ppm (Figure 20.).

The negative regions of *V(r)* from 3D electrostatic potential of 5pN-BTT in [au], were related to electrophilic reactivity and the positive ones to nucleophilic reactivity (Figure 21). The most negative *V(r)* value is associated with O8 with a value around -0.0907 a.u. while the O22 and O23 values are about -0.0799 a.u., and -0.0691 a.u., respectively. Thus, it would be predicted that an electrophile will preferentially attack 5pN-BTT molecule at the O8 position.

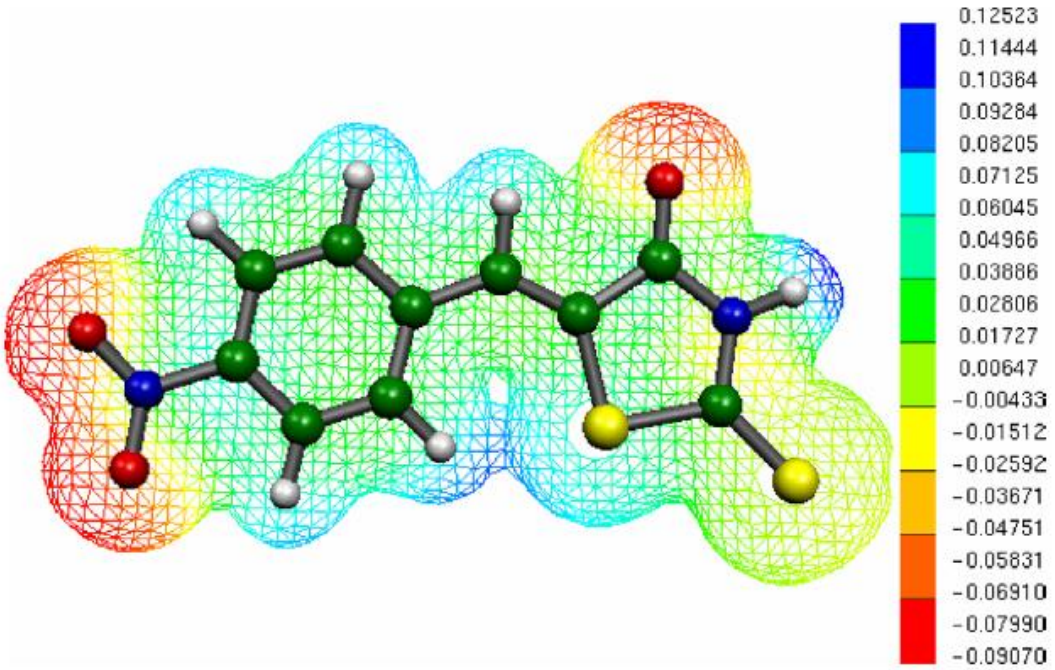

Fig. 21. Calculated 3D molecular electrostatic potential contour map of 5pN-BTT molecule in [au]. The electron density isosurface is 0.02 a.u.

Alternatively, we found a maximum value of 0.1252 a.u. on the H7 atom on the positive regions of *V(r)* indicating that this site can be the most probably involved in nucleophilic processes.

Other new compound with antimicrobial potential, structural investigated by similar experimental and theoretical methods [60] is aroyl-hydrazone 4-[2-(4-methyl-2-phenyl-thiazole-5-yl)-2-oxo-ethoxy] - benzaldehyde isonicotino – hydrazide (BINH).

Its optimized geometry and ^{1}H NMR spectrum are shown in Figures 22, 23.

The aromatic rings protons give signals in 7 – 9 ppm range: H17 and H20 multiplet at 8.052 ppm; H16, H18 and H19 multiplet at 7.577 ppm; H31 and H33 doublet at 7.123 ppm; H35 and H36 doublet at 7.714 ppm; H48 and H50 doublet at 7.824 ppm; H52 and H53 doublet at 8.789 ppm.

The singlet peak at 11.995 ppm is assigned to H41 and the singlet peak at 8.420 ppm is assigned to H39.

The protons of the methylene group give signals to 5.435 ppm and the protons of the methyl group appear at 2.785 ppm.

The values of peak integrals nicely reproduce the number of protons from each group.

To predict reactive sites for electrophilic and nucleophilic attack for the investigated compound, molecular electrostatic potential (MEP) was calculated at the B3LYP/6-31G(d) level of theory (Figure 24.).

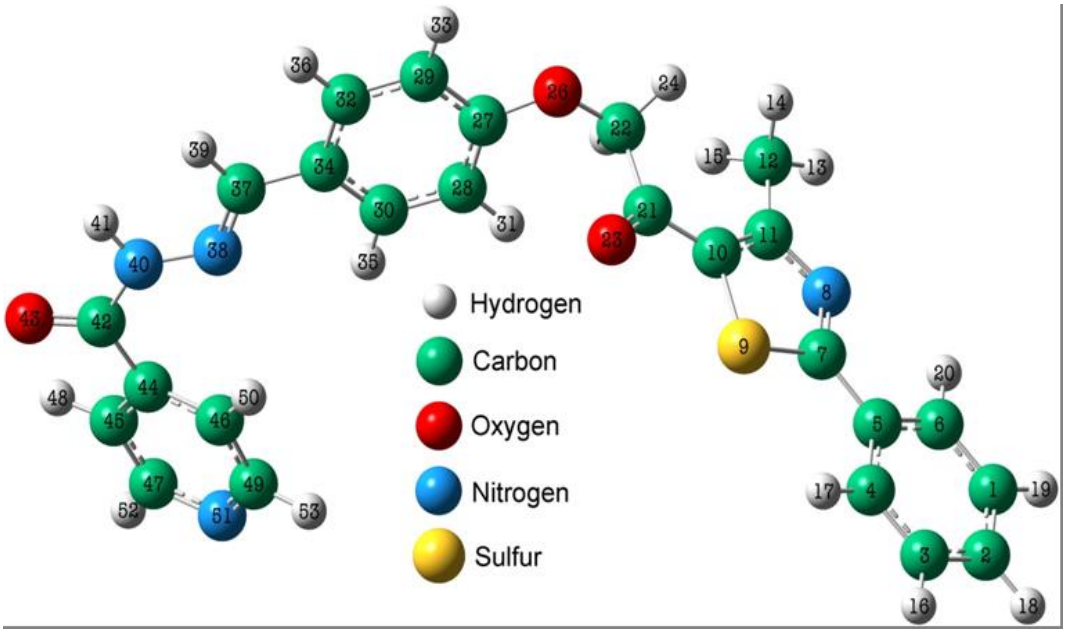

Fig. 22. The B3LYP/6-31G(d) optimized geometry of BINH molecule.

The negative regions are related to electrophilic reactivity and the positive ones to nucleophilic reactivity.

The most negative value of -0.1031 a.u. is associated with O23, O26 atoms while the values for O43 and N51 are about -0.0822 a.u., and -0.07146 a.u., respectively.

Thus, it would be predicted that an electrophile will preferentially attack this molecule at the O23, O26 positions and then the positions O43, N51.

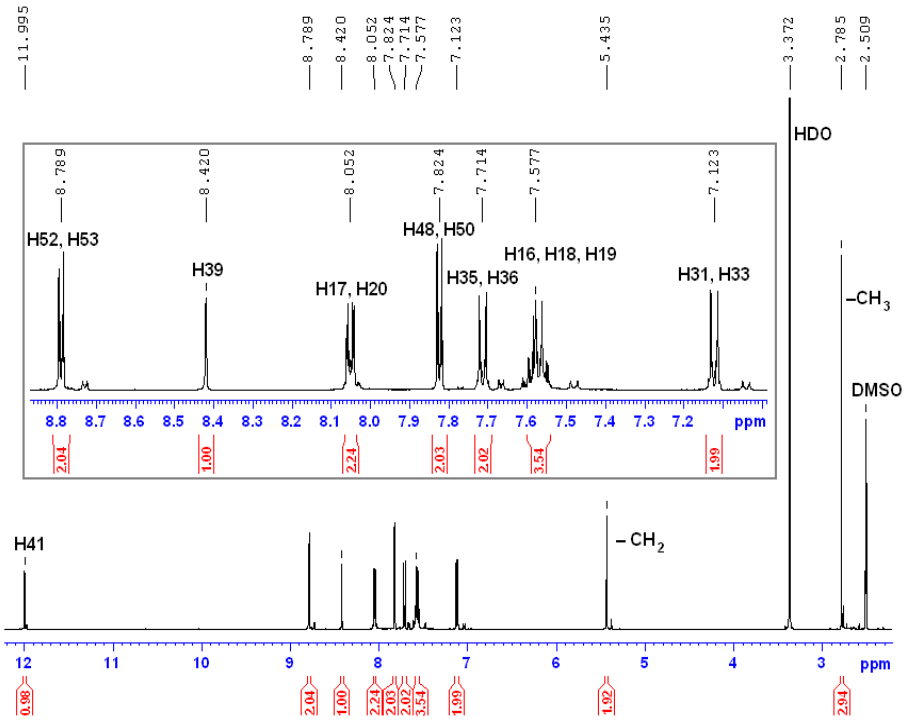

Fig. 23. [1]H NMR spectrum of BINH molecule; inset: details zoom to 7 - 9 ppm.

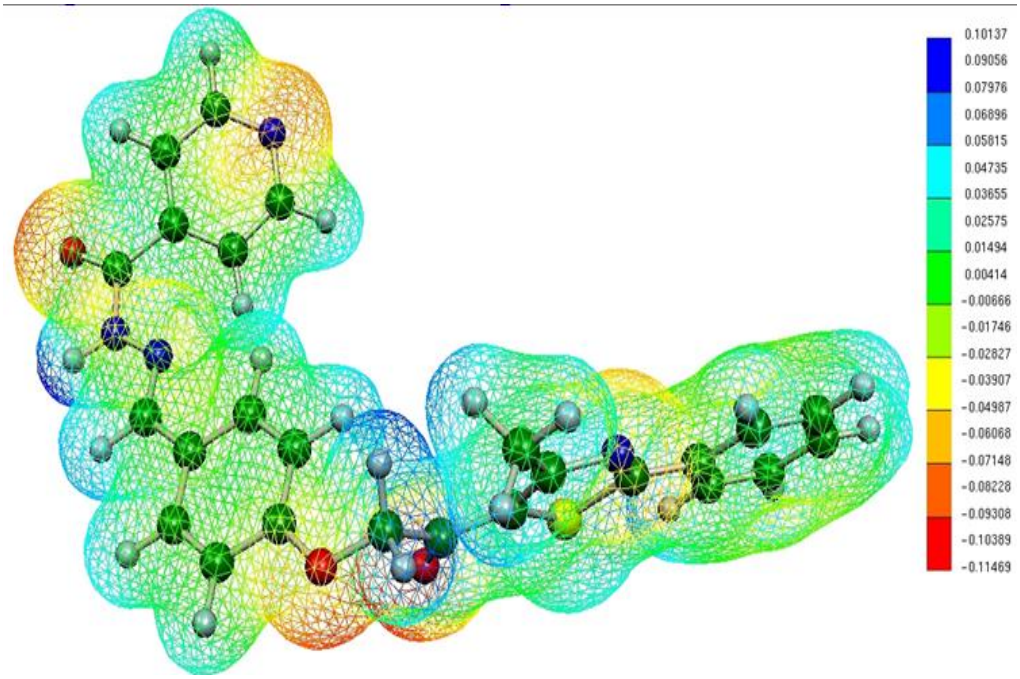

Fig. 24. B3LYP/6-31G(d) calculated 3D electrostatic potential contour map of the studied molecule (a.u.).

Alternatively, we found a maximum value of 0.04735 a.u. on the CH_2 and CH_3 groups region indicating that these sites can be the most probably involved in nucleophilic processes.

The MEP of this molecule suggests also a parallel adsorbed orientation on the silver nanoparticles by (O23, O26) the oxygen atoms and the π - electrons of rings.

Bacterial resistance has become a serious public health problem, demanding the new compounds, able to deal with resistant bacteria. In this context the potential antimicrobial 3-[2-(4-Methyl-2-phenyl-thiazol-5-yl)-2-oxo-ethyl]-thiazolidine-2,4-dione (TZD) compound was synthesized and investigated by FT-IR, FT-Raman, ^{1}H, ^{13}C NMR spectroscopies and also by DFT calculations at B3LYP/6-31G(d) level of theory [61].

The very good correlation found between the experimental and theoretical data shows that the optimized molecular structure is very close to reality. Also the NMR spectra on liquid state samples, using DMSO – d_6 as deutetrated solvent, show a monomeric behaviour of this compound in solutions.

2. Palladium (II) - theophylline compound

Several research groups have investigated the coordination of metal ions to biologically important purine derivatives - adenine and guanine, which are major constituents of DNA and RNA [16,17].

The metal complexes of N-methyl substituted xanthines – theophylline (Figure 25a) are also of major interest, because these ligands can serve as good models of biologically important analogues [62, 63].

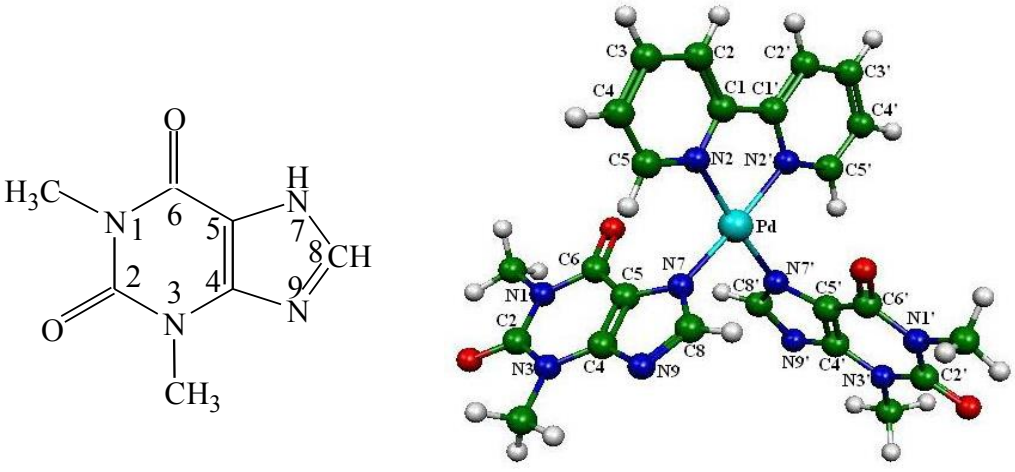

(a) (b)

Fig. 25. Theohylline structure (a) and optimized structure of $[Pd(th)_2(2,2'\text{-bipy})]$ complex (b).

Generally, the theophyllinato anion acts as a monodentate ligand, coordinating through N(7) atom to the metal ion [16,17].

The spectroscopic studies on mixed-ligand complexes of Pd(II) containing N(7)-coordinated theophylline and N,N-donor ligands like 2,2'-bipyridyne $[Pd(th)_2(2,2'\text{-bipy})] \cdot H_2O$ (Figure 25b) are present [64].

The two ν(C=O) stretching vibrations (Table 2.) are observed at lower wavenumber (1695 cm^{-1})in Pd(II) compound than in free theophylline IR spectra (1717 cm^{-1}).

This shift is mainly due to the deprotonation at the N(7) nitrogen and coordination of the theophyllinato anion through this atom to the metal centre.

The ν(C=N) vibrations of theophyline and 2,2' - bipyridine are also shifted from 1568 cm^{-1} and 1577 cm^{-1} respectively, to 1529 cm^{-1} in complex due to the coordination through N(7) atom in the case of theophylline, and N(2) and N(2') atoms in the case of 2,2'-bipyridyne at the Pd(II) ion.

Table 2. IR spectral data of theophylline, 2,2'-bipyridyne and Pd(II) compound (cm^{-1})

Compound	ν(OH)	ν(NH)	ν(CH)	ν(C=O)	ν(C=N)
Theophylline	3348 w	3122 m	2985 m	1717 s	1568 s
($C_7H_8N_4O_2$)			2825	1669 vs	
2,2'-Bipyridyne			3151-3000 m		1577 vs
($C_{10}H_8N_2$)			2925		1560 s
$[Pd(th)_2(2,2'\text{-bipy})]\cdot H_2O$	3463 w		3118-3050 w	1695 vs	1529 s
			2949	1637 vs	

The ^{1}H-NMR spectrum of theophylline shows four singlets at 13.57, 8.04, 3.44, 3.23 ppm which are accordingly assigned to N(7)H, C(8)H and the two methyl (CH_3) group protons, respectively (Table 3).

The absence of the HN(7) resonance from the ^{1}H-NMR spectrum of the complex demonstrates that theophylline coordinates in the deprotonated form.

The upfield shift of HC(8) signal by 0.36 ppm in the $[Pd(th)_2(2,2'\text{-bipy})]\cdot H_2O$ compound, is an evidence of the coordination of theophylline through the adjacent N(7) atom [64].

Table 3. ^{1}H-NMR chemical shifts data (ppm)

Compounds	**Theophylline**			**2,2' - Bipyridine**			
	N(7)H	C(8)H	CH_3	C(5)H	C(4)H	C(3)H	C(2)H/
Theophylline	13.57	8.04	3.44; 3.23				
Theophylline (DFT calc.)	7.82	7.04	3.37; 3.12				
2,2'-Bipyridyne				8.71	7.33	7.84	8.41
2,2'-Bipyridyne (DFT calc.)				8.84	6.97	7.47	7.33
$[Pd(th)_2(2,2'\text{-bipy})]\cdot H_2O$	-	7.68	3.59; 3.44	7.60	7.50	8.18	8.11
$[Pd(th)_2(2,2'\text{-bipy})]\cdot H_2O$ (DFT calc.)		6.74	3.31; 3.09	8.21	7.10	7.69	7.68

The signals of the CH_3 protons of theophylline (3.44; 3.23 ppm) are shifted downfield by 0.15 and 0.21 ppm in $[Pd(th)_2(2,2'\text{-bipy})]\cdot H_2O$, due to the hydrogen bonding involving the C=O groups from theophylline (Table 3).

The ^{1}H-NMR spectrum of 2,2'-bipyridyne shows four signals at 8.71, 8.41, 7.84 and 7.33 ppm, which are assigned to HC(5), HC(2), HC(3), HC(4) protons. Due to coordination, the resonances of HC(5) and HC(2) protons are shifted upfield (7.60 ppm and 8.11), and the resonance of HC(3) and HC(4) downfield (8.18 ppm and 7.50 ppm).

DFT optimizated structure of $[Pd(th)_2(2,2'\text{-bipy})]$ was performed with Gaussian '98 program, starting from a pre-optimized X-ray geometry in PC Spartan Pro (Figure 25b). The calculations employed the B3LYP exchange functional using LANL2DZ basis set.

In order to asses the preferred site of coordination (N7 or N9) of theophylline, the electrostatic, Mulliken and natural charges on these atoms as well as the total/relative energies of the isomers corresponding to the theophyllinato anion coordinated through N(7) or N(9) were calculated [64].

The charges on the nitrogen atoms suggest that N(9), with a higher negative charge, -0.656, -0.567 and -0.607, respectively would be the preferred coordination site. The N(9) coordinated isomer is however 114 kJ/mol higher in energy, showing that the steric congestion brought by the proximal metil group (on N3) is determinant in stabilizing the N(7) coordinated isomer.

The water molecule is hydrogen-bonded to the N(9) atoms of the theophylline rings of two adjacent $[Pd(th)_2(2,2'\text{-bipy})]$ units. The bypiridine ligands are stacked along the c-axis, the distance between the center of two benzol rings of the partially overlapped bypiridine fragments is 3.56 Å, which is the normal range for $\pi\cdots\pi$ stacking interactions (Figure. 26).

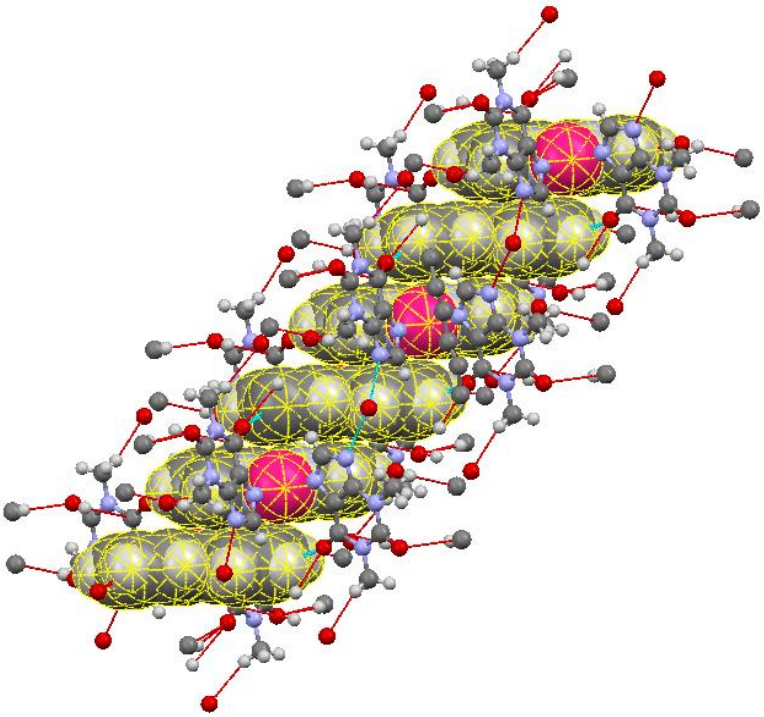

Fig. 26. The packing in the crystal of $[Pd(th)_2(2,2'\text{-bipy})]\cdot H_2O(C_6H_{12})$ emphasizing the $\pi\cdots\pi$ stacking through the bipyridine rings.

In the optimized structure (Figure 25b) the palladium ion is almost planar square coordinated by two nitrogen (N7, N7') theofilline atoms and N2, N2' atoms of bipyridine radical. Furthermore, the atoms of the 2,2'-bipyridine rings are almost coplanar and the theophyline molecules are also practically planar.

3. Copper (II) complexes with ^{15}N-labelled lysine and ornithine

The aminoacid (AA) complexes with biologically active metal ions, particularly with copper(II) have received the attention because they proved to be useful antibacterial agents, nutritive supplies for humans and animals, and also as models for metalloproteins [65].

The general coordination type for Cu(II) with two α-amino acids is the binding of both AA by an amino nitrogen and a carboxyl oxygen, i.e. a NNOO coordination or a glycine-like bonding.

Mixed-ligand complexes with two amino acids are also known to play an important role in the metal transport in the human and animal bodies.

Proteins containing amino acids with one or more of the stable isotopes of deuterium, ^{13}C, ^{15}N or ^{18}O can be used as internal standards by addition at an early stage of analysis of a complexes protein samples [66].

Labelled stable isotopes (^{15}N-lysine, ^{15}N-ornithine 99%) produced at the National Institute for Research and Development of Isotopic and Molecular Technologies, Cluj-Napoca, Romania, are used in a variety of studies, offering the ideal internal standards in quantitative information in isotopic tracers for nutrition investigations, to elucidate details of nitrogen metabolism in vivo and protein metabolism in different diseases [19,20]. All these studies demands accurate measurements of the isotopic abundances of each tracer by mass spectrometry coupled with chromatography [67] and NMR in conjunction with tracer methodologies.

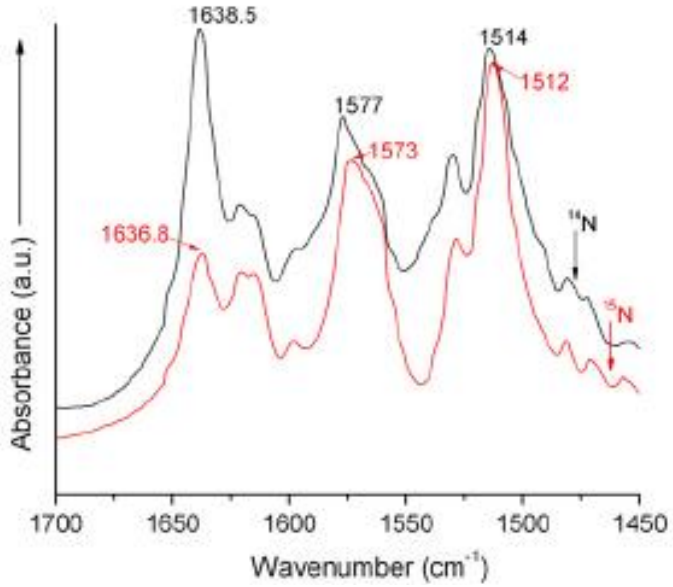

Fig. 27. FT-IR spectra of ^{14}N-lysine and ^{15}N-lysine in the 1700–1450 cm^{-1} spectral region.

The representative IR spectra [68] showing the isotopic shifts of the vibration bands of the lysine amino acids are shown in Figure 27.

The most intense bands of the lysine amino acid located in the 1700 cm^{-1}–1450 cm^{-1} region occurs at 1638.5 cm^{-1}, 1577 cm^{-1} and 1514 cm^{-1} for ^{14}N-lysine and at 1636.8 cm^{-1}, 1573 cm^{-1} and 1512 cm^{-1} for ^{15}N-lysine, respectively.

The first band is assigned to the superposition of C=O stretching, COO^- asymmetric stretching and $[NH_3]^+$ asymmetric deformation modes [69].

The last two bands (1577, 1573 cm^{-1} and 1514, 1512 cm^{-1}) are characteristics for the ^{14}N-H and ^{15}N-H bending vibrations attributed to NH_3^- asymmetric and symmetric deformations, respectively [69].

Another intense band assigned to C-N symmetric stretching vibration was observed at 1001 cm^{-1} with a very small isotopic shift (~ 1 cm^{-1}).

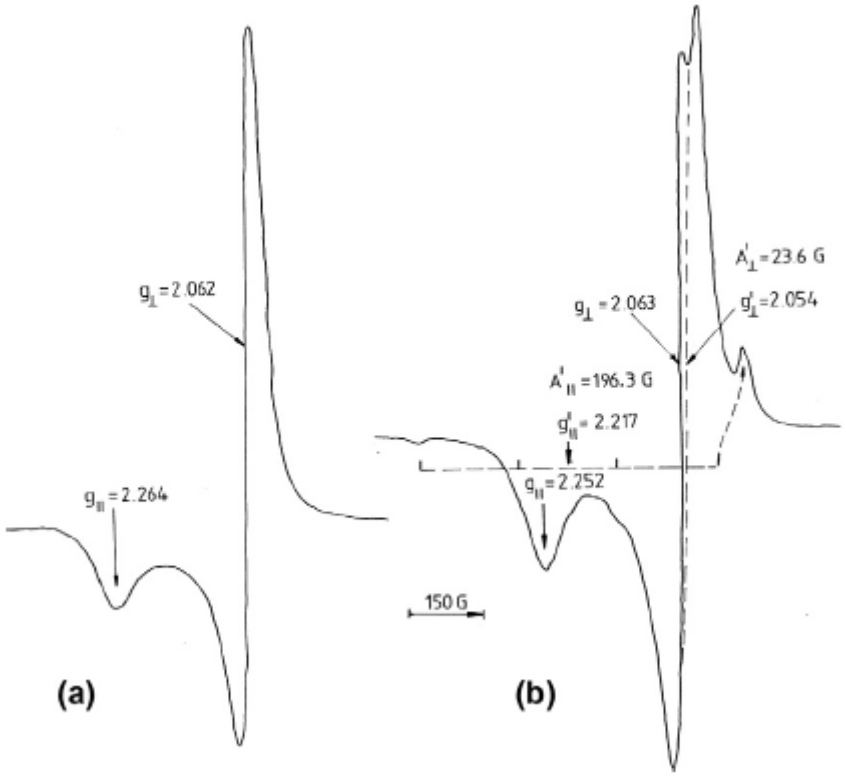

Fig. 28. Powder ESR spectra of Cu(II)–^{15}N-ornithine (a) and ^{15}N-lysine (b) complexes at room temperature.

The Cu^{2+} ion is surrounded by two N and two O atoms from the α-amino and carboxylate groups in a square-planar coordination by ligation of two lysine or ornithine molecules [70]. The powder ESR spectra of both complexes at room temperature (Figure 28) suggest the presence of dimeric species similar with that reported in the case of tetrakis (L-tyrosinato) dicopper(II) [71] and other amino acid compounds.

Generally, the deprotonated amino acid ligand acts as chelate through the N(amine) and one O atom (carboxylato), whereas the second O atom of the same carboxylato acts as bridge to the neighbouring copper (II) ion. The appearance of a weak hyperfine structure for ^{15}N-lysine compound shows the presence of monomeric impurities, too (Figure 28b).

In the case of aqueous solutions [68], the characteristic spectra of the investigated compounds show well resolved four hyperfine copper lines typical for high rate of tumbling motion (Figure 29). The three ^{15}N-superhyperfine lines (I = 1/2) due to the interaction of paramagnetic electron with two equivalent nitrogen nuclei appear clearly on the high field copper hyperfine peak (+3/2) of lysine compound (Figure 29b).

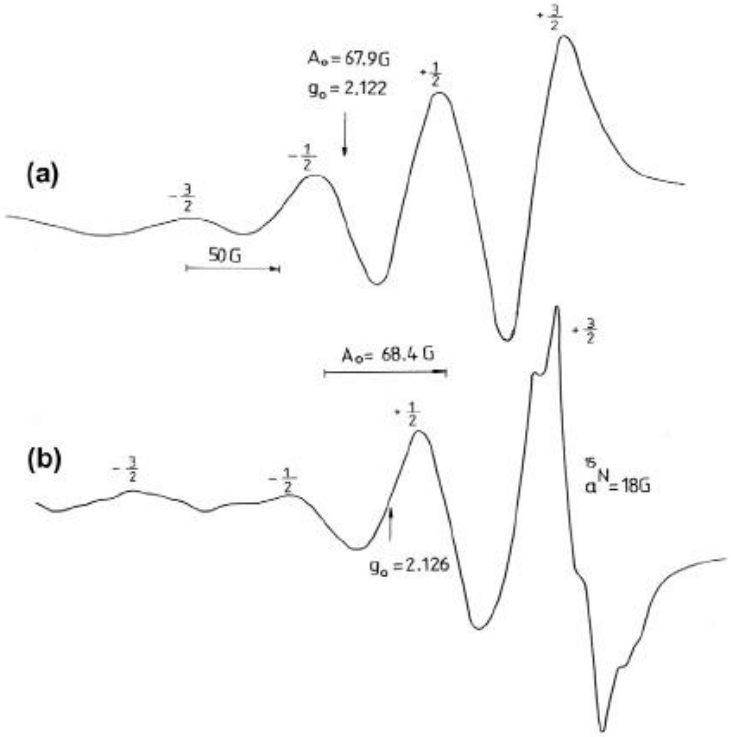

Fig. 29. Aqueous solution ESR spectra of Cu(II)–^{15}N-ornithine (a) and ^{15}N-lysine (b) complexes at room temperature.

ESR spectra of Cu(II) – ^{15}N-lysine compound adsorbed on NaY and HY zeolites are shown in Figure 30. NaY type zeolite, $Na_{56}[(AlO_2)_{56}(SiO_2)_{136}] \cdot 250H_2O$, has cavity diameters of 13 Å; (26.4%H_2O). HY type zeolite is obtained from NaY zeolite by ionic exchange of Na^+ with NH_4^+ in NH_4Cl solution at 90 ^{0}C. NH_3 is removed by heating at 500 ^{0}C, thus resulting the HY type zeolite with 13%H_2O content and cavity diameters of ~ 8 Å.

The immobilized monomeric species in the supercages of the NaY zeolite (Figure 30a) which has cavity diameters ~13 Å and an water content of 26.4%, have a tetragonal elongated octahedral symmetry due to the coordination of two water molecules at Cu $^{2+}$ ion along the O_z axis (apical positions).

These water molecules are weakly bound to copper ion and thus we can consider that $Cu(AA)_2^{2+}$ complex has practically a square-planar D_{4h} arrangement with $d_{x^2-y^2}$ ground state for paramagnetic electron ($g_{\|} > g_{\perp} > 2.0023$).

The characteristic g and A values (Table 4) of this monomeric specie evidenced in NaY zeolite are typical for CuN_2O_2 chromophore with an axial symmetry [70]. The ^{15}N hyperfine splitting observed in the $g_{\perp}$ region (Figure 30a) is of 17 x 10^{-1} cm^{-1}.

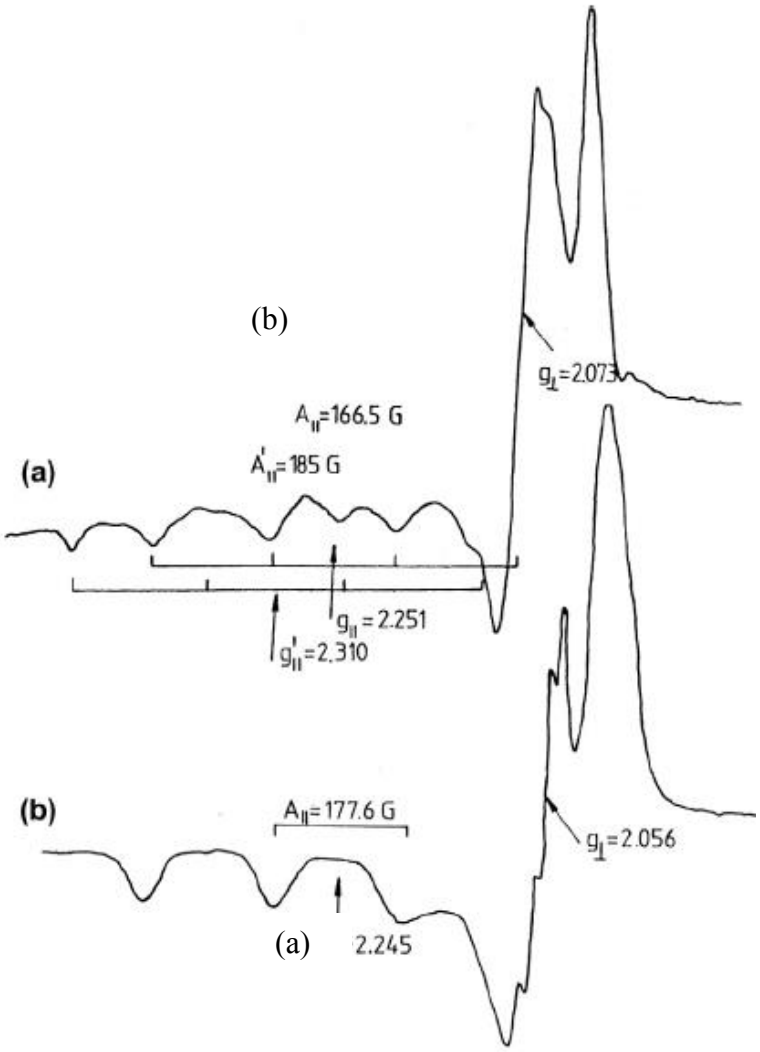

Fig. 30. Room temperature ESR spectra of Cu(II)–^{15}N-lysine compound adsorbed on NaY (a) and HY (b) zeolite.

In the case of HY zeolite with 13% water content and smaller cavity diameters (~8 Å), two different magnetically nonequivalent monomeric species were evidenced (Figure 30b). The first species having the following ESR parameters $g_{||}$ = 2.251, $A_{||}$ = 173.7 x 10^{-4} cm^{-1} for Cu(II)-^{15}N-lysine compound may be considered also immobilized in the zeolite supercages. Their local symmetry is of tetragonal–octahedral (Oh) distorted type, analogue with that from NaY zeolite. However in this case the two water molecules coordinated at Cu^{2+} ion along the Oz axis are stronger bound than in the case of NaY zeolite, leading to a real axial perturbation and to the hexacoordinated form of the metallic ions. According to the theoretical model developed by Antosik et al. [72], the g|| value is greater and

$A_{\|}$ value is smaller for the axial perturbated configuration than those characteristic of square-planar symmetry (D_{4h}) compounds, in our case the monomeric species from NaY zeolite. Using the experimental differences $\Delta g_{\|}$ and $\Delta A_{\|}$ between the values of g|| and A|| parameters for the two types of monomeric species from NaY and HY zeolites, respectively, a distance of ~2.6 Å between Cu^{2+} ion and the apical water molecules in HY zeolite was estimated [68].

The second species from HY zeolite are located on the walls of the cavities, and their $OH(OH_2)$ groups are stronger coordinated to Cu^{2+} ion than other water molecules from inner of the cavities, resulting in a slight distorted C_{4v} (square-pyramidal) local symmetry ($g_{\|} = 2.310$ and $A_{\|} \cong 200 \times 10^{-4}$ cm^{-1}).

The ESR parameter values ($g_{\|} = 2.373$, $A_{\|} = 139 \times 10^{-4}$ cm^{-1}) characteristic for monomeric species which appears in HY zeolite after a supplementary dehydration at 80^0C suggests a tetrahedral (Td) symmetry around Cu^{2+} ions [73]. In this case one or both lysine molecules are replaced by OH, H_2O groups of the support surface. The ground state for paramagnetic electron in the case of tetrahedral (Td) symmetry is d_{xy} copper orbital with an admixture of $4p_z$ copper orbital [73]. Due to the opposite contribution of the Pp and Pd dipolar terms the small values for $A_{\|}$ (100–120 G) appear in the case of Td symmetry.

From the experimental $A_{\|}$ value of this last monomeric species ($A_{\|} = 139 \times 10^{-4}$ cm^{-1}) we estimated a contribution of 2% for $4p_z$ orbital to the ground state. By using the technique described in [51] the bonding parameters characteristics of the in-plane sigma bond (α^2) and of the in-plane π bond (β^2) were estimated for each monomeric species (Table 4).

Table 4. ESR parameters of Cu(II)–^{15}N-lysine complex at room temperature

Nr. crt.	Sample	$g_{\|}$	$g_{\perp}$	$A_{\|}$	$A_{\perp}$	α^2	β^2	G	f
1	Powder	2.252	2.063					4.10	
		2.217	2.054	202.3	22.5	0.839	0.626	4.13	109.70
2	Absorbed on NaY zeolite	2.245	2.056	184.7	19	0.819	0.725	4.50	121.54
3	Absorbed on HY zeolite	2.251	2.060	173.7		0.795	0.765	4.29	129.59
		2.310	2.073	198.7		0.930	0.809	4.33	116.25
4	Absorbed on HY zeolite after suppl. dehydr.	2.373	2.075	139	19.2	0.828	0.845[4]	5.09	170.71

[4] Hyperfine parameters are given in 10^{-4} cm^{-1}.

For all these species, the in-plane σ bond has an ionic character ($\alpha^2 \cong 0.80$) while the in-plane π bond is more covalent ($\beta^2 \cong 0.73$) than that of the σ type. The values of $G = (g_{\|} - 2.0023) / (g_{\perp} - 2.0023)$ parameter which is a measure of the exchange interaction between the copper centers [74] show the presence of weak interactions ($G \cong 4$) in studied Cu(II) compounds.

The empirical factor $f = g_{\|}/A_{\|}$ [75], an index of tetragonal distortion, shows that all monomeric species from Table 4 have in principle a square-planar arrangement with small distortions ($109 < f < 120$).

The value of f increases significantly (f ≅ 170) with the appearance of tetrahedral distortion (T_d) in xOy plane for Cu(II)–Lysine compound adsorbed on HY zeolite after a supplimentary dehydration.

4. Conclusions

Performed experimental and theoretical methods used in the investigation of some biomedical compounds allowed us to obtain useful structural informations in order to a good understanding of their pharmaceutical, biological activity.

In the case metoclopramide, a gastrointestinal drug, only protonated molecular species were evidenced in aqueous solution with 3-8 pH range and both protonated and neutral species coexist in the case of adsorbtion on silver nanoparticles in the 3-11 pH range.

Based on the Raman, SERS and MEP analysis of paroxetine with anxiety and antidepressant properties an adsorbtion in a titled orientation of benzodioxol ring and perpendicular orientation on silver surface of piperidine and benzene rings were shown. Vibrational, NMR and DFT calculations proved that amlodipine, a cardiovascular drug, in a salt form with benzenesulphonate anion exist in both solid and liquid state, fact that grants its a good stability, non-hydroscopicity and processability. In the case of pindolol and verapamil, others cardiovascular drugs, were suggested that both molecules are adsorbed through the oxygen atoms and π-electrons of the rings to the silver surface in a flat and bent orientation, respectively. Vibrational data and DFT caculations shown that in the case of atenolol (ATE) and metropolol (MET) the two enantiomers (S) and (RS) exist for ATE due to the relative orientation of both acetamide and methyl-ehtyl-amino-propoxy side chains and N-protonated MET and MET-2 succinate salt, relatively exist, too. A square-planar arrangement with N_2O_2 chromophore around the copper (II) ion is realized in the case of ATE compound, while only oxygen succinate atoms are involved in the coordination of Cu–MET complex.

After experimental and theoretical investigations of antibacterial thiazolidine compound we found that from three possible tautomers, thione, thiol, enol, the most stable in water and DMSO solution is the first molecular form. Because the coordination of metal ions with theophylline can serve as good models of biologically important analogues, we establish by IR, NMR and DFT calculations that in $[Pd(th)_2(2,2'\text{-bipy})]$complex, the two theophylline molecules coordinate by two N7, N7$'$ nitrogen atoms and also by N2, N2$'$ atoms of bipyridine radical in a square planar configuration. Copper (II) complexes with ^{15}N-labelled lysine and ornithine adsorbed on NaY and HY zeolites suggest the presence of four different monomeric species with square-planar (D_4h) arrangement, tetragonal-octahedral (O_h), square-pyramidal (C_{4v}) and tetrahedral (Td) distorted symmetries.

R E F E R E N C E S

[1] T. Hesterkamp, J. Barker, A. Davenport, M. Whittaker, Curr. Top. Med. Chem., 7, 1582 (**2007**).

[2] N. Beckmann, R. Kneuer, H.U. Gremlich, H. Karmouty-Quintana, F.X. Blé, M. Müller, NMR Biomed., 20, 154 (**2007**).

[3] A. Pîrnău, V. Chis, O. Cozar, M. Vasilescu, S. Simon, J. Opt. Adv. Mater., 9, 599 (**2007**).

[4] K. Kneipp, H. Kneipp, I. Itzkan, R.R. Dasari, M.S. Feld, Chem. Rev., 99, 2957 (**1999**)

[5] S.E.J. Bell, N.M.S. Sirimuthu, Chem. Soc. Rev., 37, 1012 (**2008**).

[6] S. Cînta-Pânzaru, S. Cavalu, N. Leopold, R. Petry, W. Kiefer, J. Mol.Struct., 565, 225 (**2001**).

[7] O. Cozar, N. Leopold, C. Jelic, V. Chis¸, L. David, A.Mocanu, M. Tomoaia-Cotişel, J.Mol. Struct., 788, 1 (**2006**).

[8] R.G. Parr, W. Yang, Density-Functional Theory of Atoms and Molecules, Oxford University Press, New York, **1989**.

[9] C. Lee, W. Yang, R.G. Parr, Phys. Rev., B 37, 85 (**1988**).

[10] V. Chis, A. Pîrnău, T. Jurcă, M. Vasilescu, S. Simon, O. Cozar, L. David, Chem. Phys., 316, 153 (**2005**).

[11] V.Chiş, M.M.Venter, N.Leopold, O.Cozar, Vibrational Spectroscopy, 48, 210 (2008).

[12] N. Leopold, L. Szabo, A. Pîrnău, M. Aluaş, L.F. Leopold, V. Chiş, O. Cozar, J. Mol. Struct., 919, 94 (**2009**).

[13] E. Scrocco, J. Tomasi, Adv. Quantum Chem., 11, 115 (**1978**).

[14] N. Okulik, A.H. Jubert, Internet Electron. J. Mol. Des., 4, 17 (**2005**).

[15] A. Jubert, M.L. Legarto, N.E. Massa, L.L. Tevez, N.B. Okulik, J. Mol.Struct., 783, 34 (**2006**).

[16] T. J. Kistenmacher, D. J. Szalda and L. G. Marzilli, Inorg. Chem., 14, 1686 (**1978**).

[17] P. Bombicz, J. Madarász, E. Forizs and I. Foch, Polyhedron, 16, 3601 (**1997**).

[18] A. Stănilă, A. Marcu, D. Rusu, M. Rusu, L. David, J. Mol. Struct., 364, 834 (**2007**).

[19] F. Mesnard, R.G. Ratcliffe, Photosynth. Res., 83, 163 (2005).

[20] P.R. Grbin, M. Herderich, A. Markides, T.H. Lee, P.A. Henschke, J. Agric. Food.Chem., 55, 10872 (**2007**).

[21] T. D. Azzopardi, N. A. Brooks, Ann. Pharmacother., 42, 397 (**2008**).

[22] N.Leopold, S. Cîntă-Pânzaru, L.Szabo, D.Ileşan, V.Chiş, O.Cozar, W. Kiefer, J.Raman Spectroscopy, 41, 248 (**2010**).

[23] O.S. Palsson, J. Psychosom. Res., 69, 237 (**2010**).

[24] S.J. Mathew, R.B. Price, D.C. Shungu, X. Mao, E.L.P. Smith, J.M. Amiel, J.D. Coplan, J. Psychopharmacol., 24, 1175 (**2010**).

[25] I.B. Cozar, L.Szabo, D.Mare, N.Leopold, L.David, V.Chiş, J. Mol. Struct., 993, 243 (**2011**).

[26] P.S. Mdluli, N.M. Sosibo, N. Revrapasadu, P. Karamanis, J. Leszczynski, J. Mol. Struct., 935, 32 (**2009**).

[27] M. Muniz-Miranda, B. Pergolese, A. Bigotto, Vib. Spectrosc., 43, 97 (**2007**).

[28] S. Mishra, R.K. Singh, A.K. Ojha, Chem. Phys., 355, 14 (**2009**).

[29] S. Rohatagi, J. Lee, M. Shenouda, S. Haworth, M.S. Bathala, M. Allison, I. Rubets, R. Heyrman, R. Noveck, D.E. Salazar, J. Clin. Pharmacol., 48, 1309 (**2008**).

[30] S. Aryal, N. Skalko-Basnet, Acta Pharm., 58, 299 (**2008**).

[31] J.N. Latosińska, Chem. Phys. Lett., 463, 195 (**2008**).

[32] J.N. Latosińska, M. Latosińska, J. Kasprzak, Phys. Lett., 462, 295 (**2008**).

[33] J.M. Rollinger, A. Burger, J. Therm. Anal. Cal., 68, 361 (**2002**).

[34] S. Foley, M. Enescu, Vib. Spectrosc., 44, 256 (**2007**).

[35] L.Szabo, V.Chiş, A.Pîrnău, N.Leopold, O.Cozar, Sz.Orosz, J. Molec.Struct., 924-926, 385 (**2009**).

[36] J. Ballesteros, L.F. Callado, J. Affect. Disord., 79, 137 (**2004**).

[37] A.J. Giannini, R.S. Tarasewski, R.H. Loiselle, J. Clin. Pharmacol., 27, 980 (**1987**).

[38] I.B. Cozar, L.Szabo, N. Leopold, V. Chiş, O. Cozar, L. David, J. Molec. Struct., 993, 308 (**2011**).

[39] J.A. Creighton, Surf. Sci., 124, 209 (**1983**).

[40] M. Moskovits, J.S. Suh, J. Phys. Chem., 88, 5526 (**1984**).

[41] G.S. Schneider, J. Emerg. Med., 38, 49 (**2010**).

[42] E. Moltzer, M.F.U.S. Raso, Y. Karamermer, E. Boersma, G.D. Webb, M.L. Simons, A.H.J. Danser, A.H. van den Meiracker, J.W. Roos-Hesselink, Am. J. Cardiol., 105, 217 (**2010**).

[43] R.A. Esteves de Castro, J. Canotilho, R.M. Barbosa, J.S. Redinha, Spectrochim., Acta A, 67, 1194 (**2007**).

[44] R. Ficarra, P. Ficarra, M.R. Di Bella, D. Raneri, S. Tommasini, M.L. Calabro, A. Villari, S. Coppolino, J. Pharmaceut. Biomed. Anal., 23, 231 (**2000**).

[45] G. Bartolucci, B. Bruni, S.A. Coran, M. Di Vaira, Acta Cryst. E65, 1364 (**2009**).

[46] O. Cozar, L. Szabo, I.B. Cozar, N. Leopold, L. David, C. Căinap, V. Chiş, J. Molec. Struct., 993, 357 (**2011**).

[47] A.P. Scott, L. Radom, J. Phys. Chem., 100, 16502 (**1996**).

[48] R.G. Bhirud, T.S. Srivastava, Inorg. Chim. Acta, 173, 121 (**1990**).

[49] E. Bozkurt, B. Karabult, Spectrochim. Acta A, 73, 871 (**2009**).

[50] M. Padmanabhan, S.M. Kumary, X. Huang, J. Li, Inorg. Chim. Acta, 358, 3537 (**2005**).

[51] O. Cozar, V. Grecu, V. Znamirovschi, Electron Spin Resonance of Metal Complexes, Ed. Acad. Bucuresti, **2001**.

[52] E. Manoj, M.R.P. Kurup, A. Punnoose, Spectrochim. Acta A, 72, 474 (**2009**).

[53] Z. Wang, D.R. Powell, R.P. Houser, Inorg. Chim. Comm., 12, 511 (**2009**).

[54] I. Ucar, E. Bozkurt, C. Kazak, A. Bulut, Spectrochim. Acta Part A, 72, 11 (**2009**).

[55] C.V. Kavitha, Basappa, S. Nanjunda Swamy, K. Mantelingen, S. Doreswamy, M.A. Sridhar, J. Shashidhara Prasad, S. Rangapa, Bioorg. Med. Chem., 14, 2290 (**2006**).

[56] M.L. Cohen, Nature, 406, 762 (**2000**).

[57] A.Pîrnău, V.Chiş, L.Szabo, O.Cozar, M.Vasilescu, O.Oniga, R.A. Varga, J.Molec.Struct., 924-926, 361 (**2009**).

[58] A. Fu, H. Li, D. Du, J. Mol. Struct. (Theochem.), 767, 51 (**2006**).

[59] H. Friebolin, Basic One and Two Dimensional NMR spectroscopy, Wiley-VCH, Weinheim, **2005**, p. 60.

[60] I.B. Cozar, A. Pîrnău, L. Szabo, N. Vedeanu, C. Nastasă, O. Cozar, Rom. Journal of Physics, 61, 1265 (2016).

[61] I.B. Cozar, A. Pîrnău, L.Szabo, N.Vedeanu, C.Nasta, Rom.Rep.Phys., 68, 630 (**2016**).

[62] E. Forizs, L. David, O. Cozar, V. Chis, G. Damian, J. Csibi, J. Mol. Struct., 482, 143 (**1999**).

[63] Pneumatikakis, A. Yannopoulos, J. Markopoulos and C. Angelopoulos, Inorg. Chim. Acta., 152, 101 (**1988**).

[64] E.Forisz, A.Debreczeni, A.Patrut, A.Z. Kun, I.B. Cozar, L.David, I. Silaghi-Dumitrescu, Rev. Roum. Chim., 55, 697 (**2010**).

[65] M.Z. Iqbal, S. Khurshid, M.S. Iqbal, J. Pak, Med. Assoc., 40, 221 (**1990**).

[66] G.W. Becker, Brief. Funct. Genomic Proteonic, 7, 371 (**2008**).

[67] M. Culea, A. Iordache, C. Mesaros, Chem. Listy J., 102, 636 (**2008**).

[68] O.Cozar, I.Bratu, L. Szabo, I.B. Cozar, V. Chis, L. David, J. Molec. Struct., 993, 397 (**2011**).

[69] M.B. Mary, M. Umadevi, V. Ramakrishnan, Spectrochim. Acta Part A, 61, 3124 (**2005**)

[70] B.M. Weckhuysen, A.A. Verberckmoes, L. Fu, R.A. Schoonheydt, J. Phys. Chem., 100, 9456 (**1996**).

[71] J.F. Villa, W.E. Hatfield, Inorg. Chem., 11, 1331 (**1972**).

[72] S. Antosik, N.M.D. Brown, A.A. McConnell, A.L. Porte, J. Chem. Soc. A, 545 (**1969**).

[73] O. Cozar, I. Ardelean, J. Non-Cryst. Solids, 92, 278 (**1987**).

[74] A.E. Aliaga, I. Osorio-Roman, C. Garrido, P. Leyton, J. Carcamo, E. Clavijo, J.S. Gomez-Jeria, G. Diaz, F.M.M. Campos-Vallette, Vib. Spectrosc., 50, 131 (**2009**).

[75] E. Manoj, Biomol. Spectrosc., 72, 474 (**2009**).